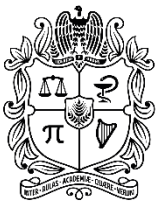

UNIVERSIDAD
NACIONAL
DE COLOMBIA

Evaluation of CO2 Flooding as an Enhanced Recovery Method in a Gas Condensate Reservoir

Gerson Orlando Rivera Ortega

Universidad Nacional de Colombia

Department of Processes and Energy

Medellín, Colombia

2019

Evaluation of CO2 Flooding as an Enhanced Recovery Method in a Gas Condensate Reservoir

Gerson Orlando Rivera Ortega

A thesis submitted in partial fulfillment of the
Requirements for the degree of
Master of Science in petroleum engineering.

Advisor:
PhD Juan Manuel Mejia Cardenas

Investigation Line:

Enhanced oil recovery

Research group: Flow and Transport Dynamics in Porous Media

Universidad Nacional de Colombia

Department of Processes and Energy

Medellín, Colombia

2019

Todo el esfuerzo y amor a mis padres quienes me ensenaron que no existen retos imposibles cuando se anhela con el corazón.

A mis hermanos, por su confianza y apoyo incondicional.

A Cesar, por su generosa escucha e inspiración.

ACKNOWLEDGEMENTS

I am thankful to Colciencias, the Colombian National Hydrocarbons Agency (ANH) and Universidad Nacional de Colombia for all the support and to make possible this study under the project '*Plan nacional para el potenciamiento de la tecnología CEOR con gas mejorado químicamente, contrato 273-2017*'

I want to thank Landmark Company for providing me NEXUS, the reservoir simulation software, key tool for conducting this project. I am very grateful with CMG for providing me the PVT simulator WinProp.

I am indebted to my advisors Dr. Juan Manuel Mejia and Juan David Valencia for the guidance and support throughout of the project.

NOMENCLATURE

Abbreviation

CO_2	Carbon dioxide	%, or Fraction
k	permeability	md
kr	Relative permeability	Fraction
krgo	Relative permeability of gas in the presence of oil	Fraction
kro	Relative permeability of oil in the presence of gas	Fraction
Swi	Initial water saturation	%, or Fraction
So	Oil saturation	%, or Fraction
Soc	Critical oil saturation	%, or Fraction
xi	Molar fraction of component i in the liquid phase	Fraction
yi	Molar fraction of component i in the vapor phase	Fraction
LDO	Liquid drop-out	%, or Fraction
API	Oil density in API units	Degrees
GOR	Gas oil ratio	Scf/stb
C7+	Heavy fraction composition	%, or Fraction
Pwf	Bottom hole pressure	Psia
Pr	Reservoir Pressure	Psia
cp	Centipoise	Cp
IFT	Interfacial Tension	mN/m
MMP	Minimum Miscibility Pressure	Psia
TBP	True Boiling Point	
CCE	Constant Composition Expansion	
MCT	Multiple Contact Test	
SPSP	Sinlge Porosity – Single Permeability	
EOS	Equation of State	
MMscfd	Millions standard cubic feet per day	
MMbbls	Millions of stock tank barrels	
HCPVI	Hydrocarbon Pore Volume Injected	
QGI	Gas Injection Rate	Mscfd
PAVH	Average Pressure weight by HC PV	psia
PBU	Pressure Build up	

Subscripts and superscripts

Variable	Unit	Name
#	script	represent a constant term, unvariable with time
n	script	temporal index representing full time step
m	index	component index, typically runs from 1..NC − 1
m'	index	primary variable component index, typically runs, from 1..NC − 2
o	script	oil phase
g	script	gas phase
w	script	water phase
i	index	spatial index in x-direction
j	index	spatial index in y-direction
k	index	spatial index in z-direction

Variables used in the mathematical formulation

Variable	Unit	Name
X_m	fraction	Mole fraction in oil phase
ξ_o	Lbmol/ft3	Molar density of oil phase
λ_o	1/cp	Mobility of oil phase (inverse viscosity)
k	md	Permeability
P_o	psi	Pressure measured in oil phase
γ_o	Psi/ft	Specific gravity of oil phase
D	Ft	Depth
Y_m	fraction	Mole fraction in gas phase
ξ_g	Lbmol/ft3	Molar density of gas phase
λ_g	1/cp	Mobility of gas phase (inverse viscosity)
P_{cgo}	psi	Gas oil capillary pressure
γ_g	Psi/ft	Specific gravity of oil phase
W_m	fraction	Mole fraction in water phase
ξ_w	Lbmol/ft3	Molar density of water phase
λ_w	1/cp	Mobility of water phase (inverse viscosity)
P_{cow}	psi	Water oil capillary pressure
q_w	Ft3/day	Water rate
q_o	Ft3/day	Oil rate
q_g	Ft3/day	Gas rate

$\emptyset$	fraction	Porosity
S_g	fraction	Gas saturation
S_o	fraction	Oil saturation
S_w	fraction	Water saturation
N_c	Unitless	Number of components
f_{om}	Psi	Oil phase fugacity of m -component
f_{gm}	Psi	Gas phase fugacity of m -component

CONTENTS

LIST OF FIGURES

CHAPTER I

INTRODUCTION

1.1 Overview

According to the Global Energy Statistical Yearbook 2019, the global energy consumption from oil and gas represented 55% of the total demand in 2018. While power generation of the renewables sources rises and become more economical, the transition requires to improve the strategies to maximize the oil and gas recovery factor. They should be implemented with minor environmental impacts as possible.

The Colombian ministry of mines and energy published that the oil reserves at the end of 2018 were 1958 MMbbls and it would cover six years of the national consumption. The demand for the Colombian gas market will be around 1370 GBTUD by 2030, according to the UPME. The reserves/production ratio for natural gas in Colombia is 13 years. These poor indicators demonstrate the importance to invest in the exploration of new fields and the execution of enhanced recovery methods.

The CO2 injection is a promising method to enhance the recovery of gas and oil fields while extensively reducing greenhouse gas emissions (Al-Abri, 2011). Since the 1970s, CO2 injection has been successfully proved as an enhanced recovery method in the U.S and several pilots around the world (Kane A.V.,1979, Oxy Denver Unit CO2 Subpart RR Monitoring, 2015, Ren, S., Niu, A., Ren, B., Li, Y., Kang, W., Chen, G. Zhang, H., 2011, China National Petroleum Corporation, 2011). In Colombia, some efforts were made in the past, and few works have been published (G. Maya, R. Castro, A. Lobo, et al., 2010, D. Rodriguez, F. Monsalve, 2009). Due to the CO2 availability, the selection of pilots, the operational problems and costs, the technology development in Colombia has been paused.

Gas condensate reservoirs are initially in the gas phase. They can supply of gas and oil according to the operational conditions of the separation system, what it is interesting for the goals of the Colombian energetical demand. This type of reservoirs exhibits a complex phase behavior which is

characterized by the condensate generation when the pressure decreases below the dew point. The problem with the condensation in the reservoir is that the liquid remains immobile due to the capillary forces until a critical liquid saturation is reached. The condensation reduces the well productivity as a new liquid phase appears in the rock, the gas flow is restricted due to the space occupied by the condensate. The relative permeability curves describe the competence between the gas and condensate for the flow.

Condensation effects in reservoir deliverability can be prevented by maintaining the pressure above the dew point or in general, as high as possible. This approach requires the injection of some fluids as lean gas, N2, or CO2.

The CO2 injection enhances the recovery of gas and condensate due to:

- The pressure support: If the pressure maintenance is executed since the beginning of the production and the reservoir pressure is kept above the dew point, condensation will not occur in the rock, and it is possible to maximize the condensate recovery at the surface. For reservoirs with pressure below the dew point, the pressure maintenance will reduce the condensation speed and mitigates the pore throat blockage that affects the well productivity.

- Condensate saturation reduction: when condensation occurs in the reservoir, the condensate will not be mobile until a critical saturation is reached. CO2 injection enhances the condensate saturation recovery due to the swelling processes (*So* increases and become mobile because of the swollen condensate volume), the viscosity reduction, the interfacial tension reduction and the vaporization of components from the condensate. The evaluation of CO2 injection into a gas condensate reservoir is the subject of this study.

1.2 Research objectives

The objective of this work is to evaluate through numerical simulation, the effects of CO2 injection in the condensate recovery factor, the reservoir pressure impacts in the recovery efficiency, the compositional changes of the produced fluids and the production mechanisms. The specific objectives can be summarized as follows:

1. Validate an EOS model with experimental phase behavior data of reservoir fluids and CO2.
2. Evaluate the effects of CO2 injection rates in the condensate recovery factor in a hypothetical gas condensate reservoir through numerical simulation.
3. Evaluate the impact of the reservoir pressure in the performance of CO2 injection through sensitivities in the starting of the CO2 injection.

CHAPTER II

LITERATURE REVIEW

2.1 Gas condensate reservoirs

According to Whitson (2000), the classification of a reservoir fluid could be done by identifying:

1. The reservoir temperature in the P-T diagram concerning the critical and the cricondentherm temperatures.
2. The separator conditions in the P-T diagram.

The temperature of the gas condensate reservoirs is higher than the critical temperature and less than the cricondentherm (B point in *Figure 1*). The first stage of the separator conditions is located in the 2-phases region (A2 point). These reservoirs are commonly found in the range of 3,000 - 10,000 psi and 200 - 400 °F (Roussennc, 2001).

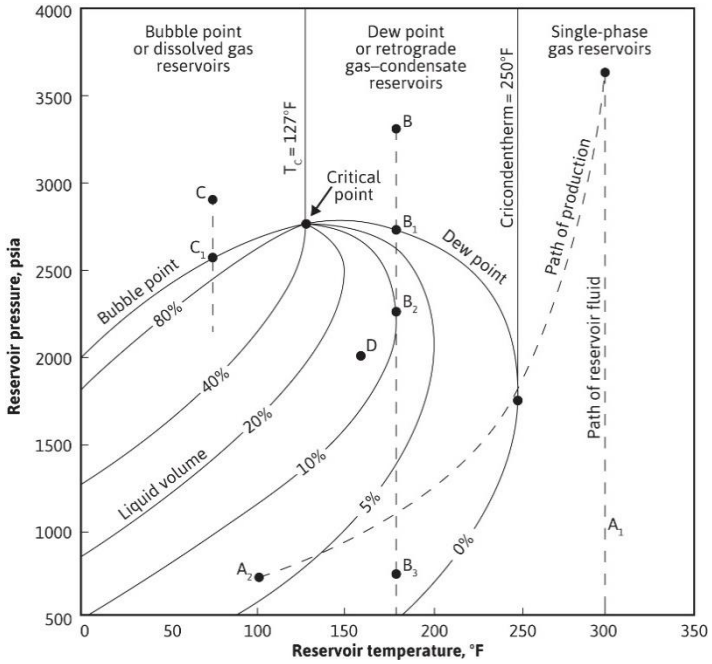

Figure 1. Phase envelope of a gas condensate reservoir. Source: Terry, Ronald E., J. Brandon. Rogers, and B. C. Craft. Applied Petroleum Reservoir Engineering. Third ed. Massachusetts: Prentice Hall, 2014. Print.

Once the production starts, the reservoir pressure decrease at an isothermal condition. When the saturation pressure is reached, the liquid hydrocarbon is generated. The liquid drop-out starts to increase as the reservoir depletion is more significant (*Figure 2*). The quantity of liquid hydrocarbon depends on the depletion degree and the gas condensate composition. Further pressure depletion will increase the liquid drop-out until a maximum value; then the liquid starts to be vaporized.

The problem with the condensation in the reservoir is that the condensate remains immobile due to the capillary forces until a critical liquid saturation is reached. The well productivity is reduced as a new phase appears in the rock, the gas flow is restricted due to the space occupied by the condensate. The competence for the flow is described with the relative permeabilities curves as presented in *Figure 3*.

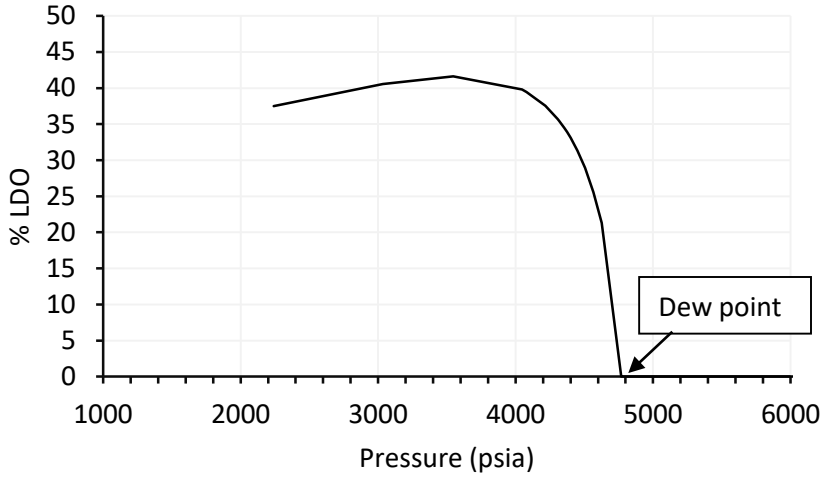

Figure 2. Liquid drop-out of a gas condensate reservoir.

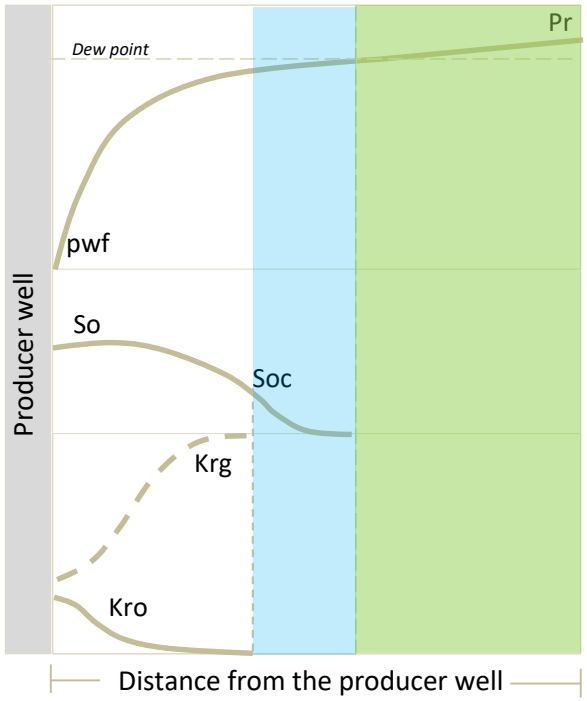

Figure 3. Condensate saturation profile and relative permeability curves concerning the pressure depletion in a gas condensate reservoir.

Three fundamental forces control the flow of gas and condensate in the porous media: capillary, gravitational, and viscous forces. Within the reservoir where the flow velocities are low, the capillary and gravitational forces rule the flow. In the near-wellbore, where high velocities are found due to the higher drawdown and reduced flow area, the flow is dominated by the viscous and capillary forces (Ursin, 2004).

According to Fevang and Whitson, 1995; Ali et al.1997; Gringarten and Al-Lamki, 2000, three regions could be identified in a gas condensate reservoir when the bottom hole pressure is below the saturation pressure (*Figure* 4):

I Region: located far from the producer well. In this zone, the reservoir pressure is above the saturation pressure; only the gas phase is present and it flows slowly. This region will eventually disappear as the depletion increases and the pressure reaches the dew point.

II Region: the outer boundary is the distance in the reservoir where the pressure is just below the dew point, at this region the liquid hydrocarbon is formed and start the competence for the space to flow. The inner boundary is the distance in the reservoir where the condensate saturation is about to reach the critical saturation. Under this condition, only gas flows and it loses some heavier components in the immobile liquid phase.

III region: it is the closest region to the well in which the pressure is as low that the condensate reaches the critical saturation and the two phases can flow at constant composition.

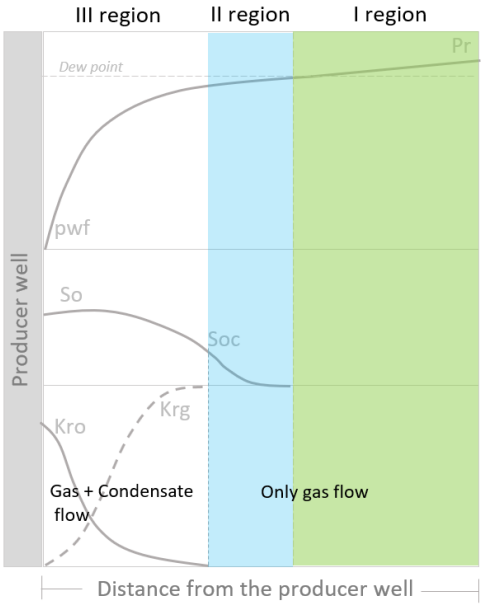

Figure 4. Flow regions in a gas condensate reservoir concerning the distance from the producer well.

The typical composition of a gas condensate reservoir has a heavy fraction between 6% < C7+ <12.5% molar, API in the range of 40-60 and GOR between 3,200 - 150,000 scf/stb (Whitson, 2000). The GOR remains constant until the saturation pressure is reached; further depletion will increase the GOR as the condensate remains immobile in the reservoir.

To prevent the impacts of the condensation in the reservoir is recommended to maintain the reservoir pressure above the dew point or at least as higher as possible, this approach requires the injection of some fluids as lean gas, N2 or CO2. Once the condensation is present, the damage could be mitigated by changing the phase behavior of the reservoir fluids with some treatments as methanol, using chemicals to reduce the interfacial tension, executing hydraulic fracturing or injecting lean gas or CO2 (Henderson et al., 1991, Li and Firoozabadi, 2000).

2.2 The Principles of CO2 injection as an enhanced recovery method.

CO2 Injection is an enhanced recovery method, usually preceded of primary production and waterflooding projects; the objective is to recover the remaining oil by contacting, vaporizing and mobilizing non-swept oil. CO2 injection has been historically implemented in medium to light oils (API >28°, viscosity < 3 cp).

CO2 injection derives in several displacement mechanisms, including solution gas drive, immiscible displacement, multi-contact miscible, and miscible (Brown, 2014). Most reservoir rock types, including sandstones and carbonates, are suitable for CO2-EOR application provided good reservoir connectivity is present.

The main CO2 recovery mechanisms are related to (Holm and Josendal, 1974. Tabrizy, 2012):

I. Oil swelling, It can increase the oil volume by 10-50% (Klins and Farouq Ali, 1984). The swollen oil ejects the oil volume around it and increases the oil saturation.
II. Viscosity reduction. CO2 improves the mobility ratio and sweep efficiency.
III. The generation of Carbonic acid when CO2 is dissolved in water (for carbonate rocks). It increases the porosity and stabilizes the clays in shaly formation, which also increases the injectivity (Holm and Josendal, 1974).
IV. IFT reduction and miscibility.
V. Vaporization of lighter components from the oil.
VI. Reservoir pressure support.

The CO2 critical pressure and temperature are 1070,6 psia and 31,1°C, respectively. At higher conditions (most field cases), the density becomes like that of a liquid and viscosity remains like that of a gas. The miscibility of the supercritical CO2 with the contacted oil improves the fluid phase behavior and increase the sweep efficiency.

The understanding of HC/CO2 phase behavior has a strong impact (Grigg and Schechter, 1997) on the simulated benefits of the CO2-EOR and in general for all gas injection processes. Phase behavior directly affects the recovery efficiency (Whitson, 2000):

I. Viscosities affect the mobility ratio and so the areal and vertical sweep efficiency.

II. The phase densities control the segregation degree, affecting the vertical sweep efficiency.
III. Interfacial tensions and miscibility affect the residual oil saturation and so the microscopic displacement efficiency.

To understand the behavior of the fluids, engineers can use tuned Equations of State (EOS) with especial PVT fluid studies as swelling tests, multi-contact tests, MMP & IFT measurements.

Miscible injection typically yields higher recoveries than immiscible processes. The driving criteria is to inject CO2 above the MMP (minimum miscibility pressure), in which CO2 and the contacted fluid form a single phase. MMP is defined as the pressure where 90% of the recovery factor is reached when 1,2 HCPV of CO2 is injected. MMP is estimated via slimtubes tests or IFT measurements.

According to Holm and Josendal, high content of C5-C12 in the oil decreases the MMP. Aromatic oils have in general a lower MMP in comparison to the paraffinic oils. The mix of CO2 with methane, N2 and C2-C4 fractions have a significant effect on the MMP. C1 & N2 tend to increase MMP, whilst C2-C4 tend to reduce the MMP.

The CO2 miscibility mechanisms are described in *Figure* 5 (Stalkup, 1983).

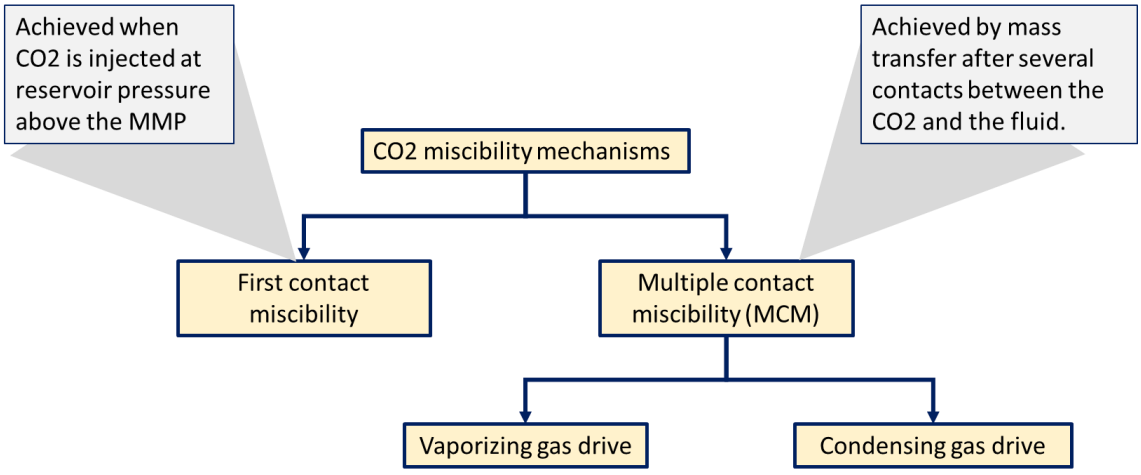

Figure 5. CO2 miscibility mechanisms. Author

In vaporizing gas-drive, the mass transfer occurs when the gas contacts the oil extracting light and intermediate components; the gas become richer (Danesh, 1998). In condensing gas-drive, the

contact between the rich gas and the oil yields mass transfer by condensing of some fractions of intermediate components into the oil. *Figure* 6 shows a schematic of miscible CO2 flooding.

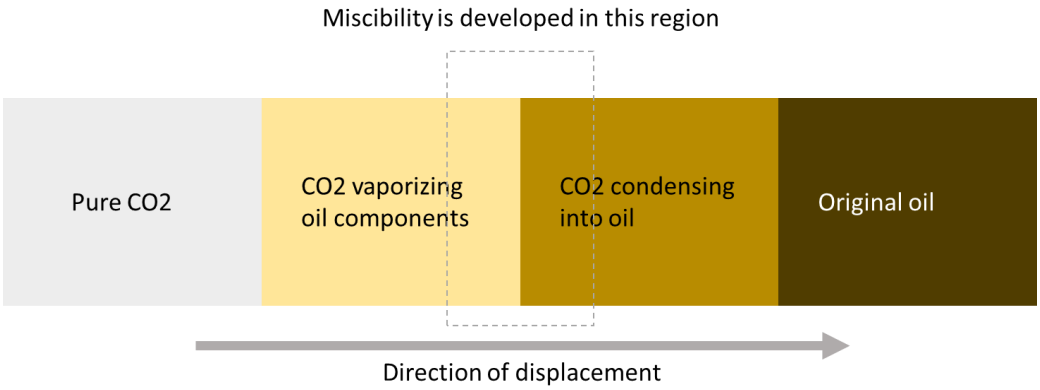

Figure 6. Schematic of the miscible CO2 flooding process (adapted from Holm and Josendal, 1974).

Although miscible conditions are desirable, the immiscible CO2 improves the oil mobility by swelling and reducing the viscosity. CO2 can reduce in several orders of magnitude the viscosity of high viscosity oils. Low-pressure reservoirs and reservoirs with API <30° are typical candidates for immiscible CO2 displacement (Whitson, 2000).

The CO2 injection can be continuous, alternated with water (CO2-WAG) or Huff and Puff type. WAG is a standard method to improve sweep efficiency. CO2 injection is performed in patterns (Verma, 2015), being the most widely used the five-spots, inverted five-spots, and in some cases, seven- or nine-spots patterns.

There are mathematical formulations to simulate the solubility of CO2 in water (Chase and Todd, 1984) included in some commercial software. CO2 solubility in water may affect the recovery efficiency if there is a loss of CO2 into the remaining contacted water.

CO2 injection can cause asphaltenes precipitation. That can block the porous throats sizes thus reducing productivity or injectivity of the wells as observed by Monger & Trujillo during CO2 flooding tests.

When dealing with naturally fractured reservoirs, there is another mass transport mechanism to be considered which is molecular diffusion. Darvish (2007) presented an experimental study in a chalk core to reproduce the phenomenon; CO2 was injected into the core with an annular setting to emulate the natural fracture effect. The experiment was simulated with the conventional formulations, but it could not reproduce the final recovery factor due to the prediction of an accelerated recycling process. When the simulation included the molecular diffusion model of Leahy-Dios and Firoozabadi, the results matched the experimental data (*Figure* 7).

Darvish explains the occurrence of mass flux between the CO2 that flows through fractures and the fluids in the matrix due to differences in chemical potential. This mass exchange promotes an improvement in the phase behavior of the contacted fluid and lets it flow easily.

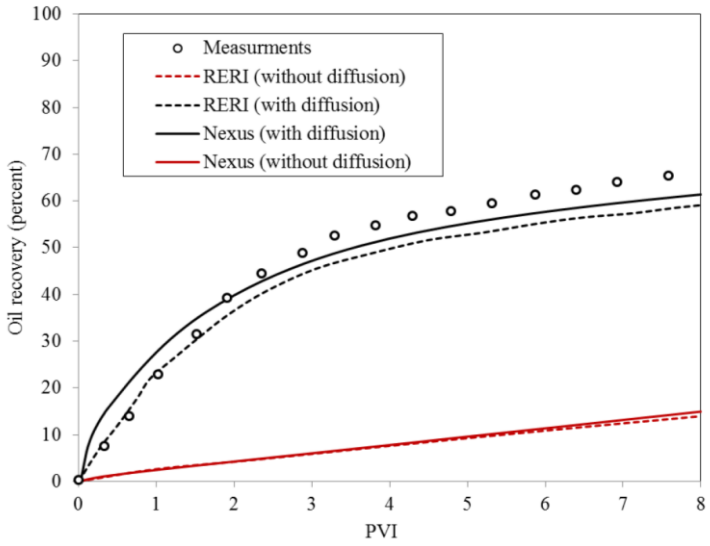

Figure 7. Simulation of a CO2 flooding experiment, with and without Molecular diffusion. Darvish 2007.

CO2 injection into gas condensate reservoirs

The CO2 injection is a promising method to enhance the recovery of gas and condensate due to:

- The pressure support: If the pressure maintenance is executed from the beginning of the production and the reservoir pressure is kept above the dew point, condensation will not occur in the rock, thus maximizing the condensate recovery at surface. For reservoirs with pressure below the dew point, the pressure maintenance will reduce the condensation rate and mitigates the pore throat blockage, which affects the well productivity.

- Condensate saturation reduction: when condensation occurs in the reservoir, the condensate will not be mobile until a critical saturation is reached. An important part of it will remain unrecoverable due to the capillary forces. CO2 injection enhances the condensate saturation recovery due to the swelling processes (Condensate saturation increases and become mobile because of the swollen condensate volume), the viscosity reduction, the interfacial tension reduction, and the vaporization components from the condensate.

2.3 Modeling CO2 injection

The simulation of gas injection processes like the miscible or immiscible CO2 flooding requires the use of a fully compositional multiphase flow model in porous media. The complexity of the fluids phase behavior and the compositional changes is reproduced with the use of Equations of State (EOS) (Aziz & Settari 1979, Chavent & Jaffre 1986, Danesh 1998, Firoozabadi 1999)

The compositional reservoir simulation must represent the simultaneous transport of all described components in all possible phases in the porous media. It involves solver a large system of non-linear equations arising from the discretization of partial differential equations (PDEs) for modeling the fluid flow (Schmall, L., Varavei, A., & Sepehrnoori, K. 2013). The mathematical model presented in this document is one of the many possible formulations.

The general formulation to describe the fluid flow involves the mass balance equations, flow formulations, and the equation of state:

The mass balance formulation for an infinitesimal element during a time interval is as follows:

$$\begin{bmatrix} Quantiy \\ of\ mass\ in \end{bmatrix}_{\Delta t} - \begin{bmatrix} Quantiy \\ of\ mass\ out \end{bmatrix}_{\Delta t} \pm \begin{bmatrix} Quantity\ of \\ mass\ by\ sources \\ or\ sinks \end{bmatrix}_{\Delta t} = [Acummulation]_{\Delta t}$$

Equation 1. Mass balance concept.

The mass balance is done for each described component and coupled with flow equations and fluids properties. The following set of equations describes the differential equations used to solve compositional flow in a porous medium (Brown, 2014). For all components (Nc), the mass balance is:

$$\underbrace{\begin{bmatrix} Quantiy \\ of\ mass\ in \end{bmatrix}_{\Delta t} - \begin{bmatrix} Quantiy \\ of\ mass\ out \end{bmatrix}_{\Delta t}}_{}$$

$$\begin{aligned} 0.006328\,\nabla\cdot\left(X_m\xi_o\lambda_o k(\nabla P_o-\gamma_o\nabla D)\right)+\ 0.006328\,\nabla\cdot\left(Y_m\xi_g\lambda_g k\left(\nabla P_o-\nabla P_{cgo}-\gamma_g\nabla D\right)\right) \\ +\ 0.006328\,\nabla\cdot\left(W_m\xi_w\lambda_w k(\nabla P_o-\nabla P_{cow}-\gamma_w\nabla D)\right) \\ +\ \underbrace{\left(X_m\xi_o q_o+Y_m\xi_g q_g+W_m\xi_w q_w\right)}_{\begin{bmatrix} Quantity\ of \\ mass\ by\ sources \\ or\ sinks \end{bmatrix}_{\Delta t}} = \underbrace{\frac{\partial}{\partial t}\left(\emptyset\left(X_m S_o\xi_o+Y_m S_g\xi_g+W_m S_w\xi_w\right)\right)}_{[Acummulation]_{\Delta t}} \end{aligned}$$

Equation 2. Differential equations used to solve compositional flow in a porous medium for Nc components.

The symbol ∇ denotes the divergence to simplify the expression:

$$\nabla = \frac{\partial}{\partial x} i + \frac{\partial}{\partial x} j + \frac{\partial}{\partial x} k$$

Equation 3. Divergence meaning.

The molar constraints are defined as:

$$\sum_{m}^{Nc-1} X_m = 1 \rightarrow X_{Nc-1} = 1 - \sum_{m'}^{Nc-2} X_{m'}$$

$$\sum_{m}^{Nc-1} Y_m = 1 \rightarrow Y_{Nc-1} = 1 - \sum_{m'}^{Nc-2} Y_{m'}$$

Equation 4. Molar constraints

As water is not considered to be part of the hydrocarbon liquid and gas phases, the upper limit of the sums are Nc-1 and not Nc.

For H2O component, the general equation is simplified, considering it is present in the aqueous and CO2 phases:

$$0.006328\, \nabla \cdot \left((1 - W_{CO2})\xi_w \lambda_w k(\nabla P_o - \nabla P_{cow} - \gamma_w \nabla D)\right) + \left((1 - W_{CO2})\xi_w q_w\right) = \frac{\boldsymbol{\partial}}{\boldsymbol{\partial t}}\left(\emptyset(\mathbf{1} - \boldsymbol{W_{CO2}})\boldsymbol{S_w}\boldsymbol{\xi_w}\right)$$

Equation 5 Differential equation used to solve compositional flow in a porous medium for H2O.

The thermodynamic constraints represent the equilibrium conditions between the liquid and gas hydrocarbon phases. There are Nc-1 thermodynamic constraints evaluated at time n+1. Thermodynamic equilibrium is reached when the fugacity of the hydrocarbon liquid phase is equal to the fugacity of the hydrocarbon gas phase, as follows:

$$\boldsymbol{f_{om}^{n+1} = f_{gm}^{n+1}}$$

Equation 6. Fugacity constraint.

The fugacity is calculated based on the equation of state (e.g.. Peng Robinson Equation of State).

Saturation constraint is expressed by:

$$S_o + S_g + S_w = 1$$

Equation 7. Saturation constraint.

Solution Strategy for the differential equations

Once the formulations are described, they must be solved simultaneously for each grid block (Schmall, L., Varavei, A., & Sepehrnoori, K.). The solution is obtained via numerical methods due to the non-linearity of the differential equations. There are several methods to approach the derivative solution; depending on the reference time for the solution of each term; they could be implicit or explicit. In general, Explicit approach solves in t=n and requires initial and boundary conditions. The implicit approach solves in t=n+1, and an equations system is created to be solved simultaneously.

The solution strategy considers classifying the unknown variables into primary or secondary variables. The primary variables are solved first, and the secondary variables calculated subsequently. Due to the number of unknown variables, different sets of them could be selected as primary or secondary, and so many solutions are possible.

The most common approach is to consider pressure, saturation, and molar fractions as the primary variables (Coats, 1980).

In the IMPES method, P is solved implicit (time= n+1) and explicit saturation. In the IMPSEC formulation, both pressure and saturation terms in the spatial derivatives are calculated in t=n+1 and explicit composition (the basic idea of this method is to reduce the system of equations (2Nc+6) per grid block (Rodriguez, F. & Galindo-Nava, A. 1994). In the FULLY IMPLICIT formulation, all primary variables are solved at t=n+1.

According to Brown (2014), the IMPES formulation is computationally very efficient. The IMPSEC formulation captures additional variability in the saturation with the possibility of larger stable time steps. A fully implicit method is computationally inefficient.

IMPES formulation in finite differences of ***Equation 2*** is:

$$
\begin{aligned}
0.006328\,\nabla\cdot\left(\frac{{X_m}^n{\xi_o}^n}{\mu_o^n}k_{ro}^n k^{\#}\left(\nabla {P_o}^{n+1}-{\gamma_o}^n\nabla D^{\#}\right)\right)+\ 0.006328\,\nabla \\
\cdot\left(\frac{{Y_m}^n{\xi_g}^n}{\mu_g^n}k_{rg}^n k^{\#}\left(\nabla {P_o}^{n+1}+\nabla {P_{cgo}}^n-{\gamma_g}^n\nabla D^{\#}\right)\right)+\ 0.006328\,\nabla \\
\cdot\left(\frac{{W_m}^n{\xi_w}^n}{\mu_w^n}k_{rw}^n k^{\#}\left(\nabla {P_o}^{n+1}+\nabla {P_{cow}}^n-{\gamma_w}^n\nabla D^{\#}\right)\right) \\
+\ \left({X_m}^n{\xi_o}^n{q_o}^n+{Y_m}^n{\xi_g}^n{q_g}^n+{W_m}^n{\xi_w}^n{q_w}^n\right) \\
=\frac{1}{\Delta t}\left(\emptyset^{n+1}\left({X_m}^{n+1}{S_o}^{n+1}{\xi_o}^{n+1}+{Y_m}^{n+1}{S_g}^{n+1}{\xi_g}^{n+1}+{W_m}^{n+1}{S_w}^{n+1}{\xi_w}^{n+1}\right)\right) \\
-\frac{1}{\Delta t}\left(\emptyset^{n}\left({X_m}^{n}{S_o}^{n}{\xi_o}^{n}+{Y_m}^{n}{S_g}^{n}{\xi_g}^{n}+{W_m}^{n}{S_w}^{n}{\xi_w}^{n}\right)\right)
\end{aligned}
$$

Equation 8. IMPES formulation for solving differential equations for Nc components.

CHAPTER III

NUMERICAL SIMULATION OF CO2 FLOODING INTO A GAS CONDENSATE RESERVOIR

3.1 Reservoir model description and assumptions

A hypothetical simulation model was created using the information of a Colombian gas condensate reservoir.

The reservoir is composed by folded and overlapped tight sandstone formations characterized by a very low matrix permeability (~0.1md in average), porosities of around 4% and natural fractures systems which enhance wells productivity. The model includes six main compartments for the principal structure with partial communication between some of them.

Although the simulations were run using a full-field model, the scope of the work was focused on evaluating the CO2 injection pilot in a single formation, called M sand henceforth. The grid used for the simulations was non-orthogonal and non-structured comprising 178 x 26 x 10 cells and modeled as single porosity and single permeability.

The matrix permeability varies from 0.002 to 2.8 md. To consider the permeability improvement due to natural fractures system, a new matrix-fracture permeability model was created using multiple PBU interpretation results. *Figure 8* shows the matrix-fracture permeability distribution for the M sand.

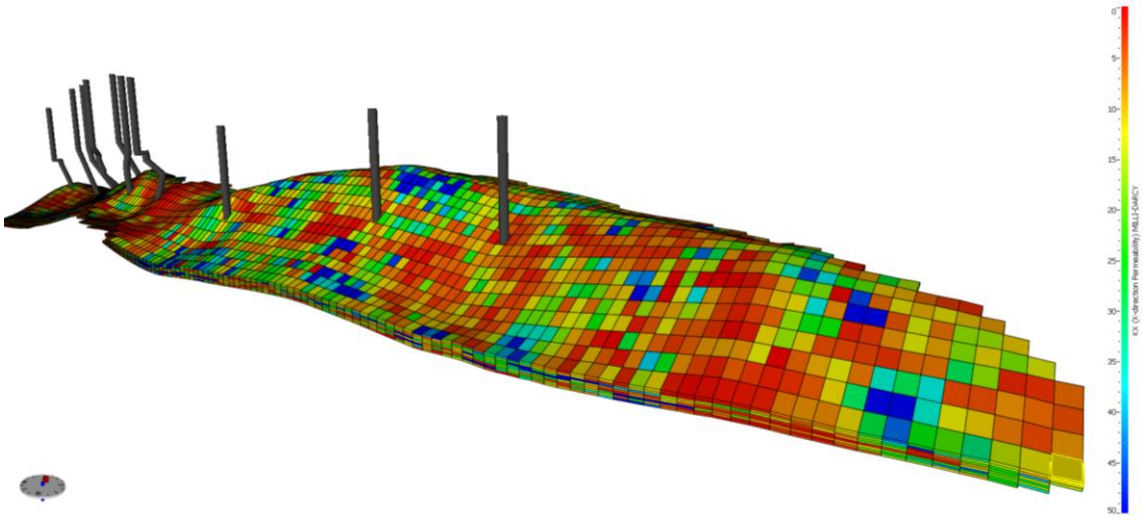

Figure 8. Permeability model (Matrix + Fracture).

The objective of using the full field model instead of a sector model was to understand the incremental oil benefits due to the recycling processes and regional pressure maintenance. Thus, incremental oil is not only expected in the primary producer well but also at field level.

The study was conducted for a gas condensate field evidencing the presence of compositional gradients from gas condensate in the crest to volatile oil in the flanks for M sand.

A fluid description was done in the past considering basic PVT and vaporizing studies with lean gas; it resulted in a 12 pseudo-components EOS tuned with the available experimental data. Several compositions versus depth tables were created to represent the compositional grading; they were used for initializing the different reservoir compartments. The initial reservoir pressure was 6600 psi at 13400 ft TVDSS, and the saturation pressure varies from 5400 – 6400 psi due to the compositional variation with depth. *Table 1*. summarizes the reservoir model description.

Table 1. Reservoir model description

Reservoir model description	
Lithology	Sandstone
Grid	178 x 26 x 10
Grid block size (ft)	500 x 500 x 70
Grid model	Single porosity and single permeability
Average matrix permeability md	0.1
Average porosity %	4%
Datum pressure (psi)	6600
Datum temperature (°F)	260
Fluid type	Gas condensate
OOIP (MMbbls)	154
Aquifer type	Numerical (weak aquifer)
Simulation end date	Dec-2035
Datum composition	
Pseudocomponent	Molar fraction
CO2	0.0340
N2	0.0055
C1	0.7263
C2	0.0803
C3	0.0406
C4	0.0251
C5-6	0.0196
C7-10	0.0358
C11-14	0.0138
C15-20	0.0111
C21-29	0.0056
C30+	0.0022

The field has been produced under lean gas injection with partial voidage. A significant quantity of gas is sold, and depletion increases rapidly. Historically, the gas injection in the M sand was focused at the center and north region of the structure due to the facility infrastructure. Thus, the derived development strategy led to negligible pressure support to the south of the structure, causing condensate banking and water intrusion from the aquifer.

The M sand has two injector wells and eight producer wells. Due to the lack of gas injection in the south zone of the reservoir and the relatively low recovery factor, the zone was selected to evaluate the effects of CO2 flooding through numerical simulation.

For estimating the final oil recovery factor after the deployment of the different strategies, a report region was created in the south of the structure as depicted by *Figure 9*. The Well-7 was evaluated as CO2 injector while the Well-5 was the principal producer in the project due to the proximity to the injector (2.3 km).

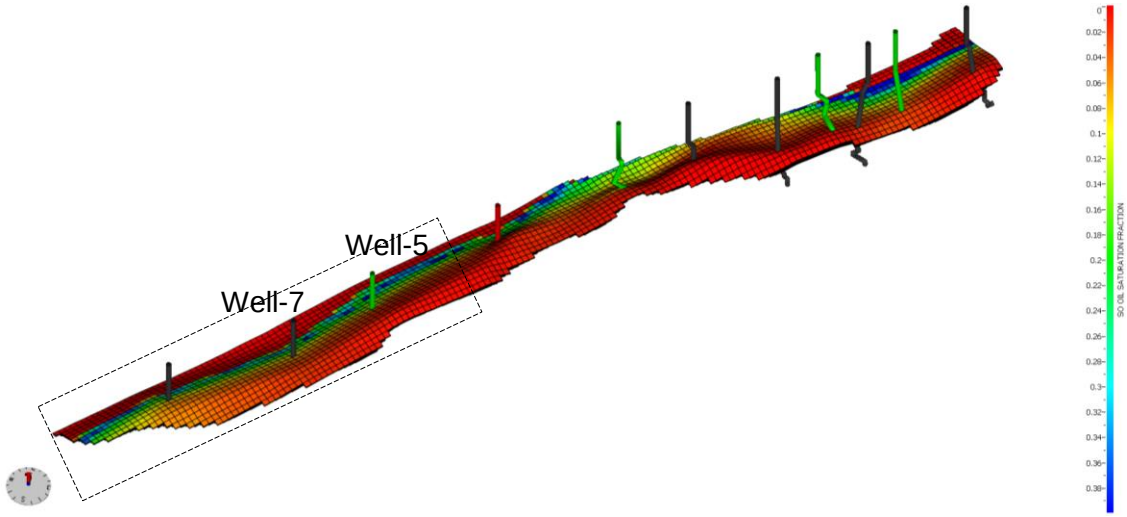

Figure 9. Simulation region for report purposes.

Assumptions

- Non-Darcy flow effects were considered.
- Single porosity single permeability grid (SPSP).
- No molecular diffusion was considered as SPSP was used.
- Compositional gradients considered.
- Constant CO2 injection rates simulated.
- The gas sale is included and it is unaffected for the incremental composition of CO2 in the gas stream after the breakthrough.
- Full-field gas reinjection is considered, CO2 is injected only in Well-7.

3.2 Specialized PVT studies for CO2 modeling.

The simulation of gas injection processes like the miscible or immiscible CO2 flooding requires the use of a fully compositional multiphase flow model in porous media. The complexity of the fluids

phase behavior and the compositional changes is modeled through Equations of State (EOS) (Aziz & Settari 1979, Chavent & Jaffre 1986, Danesh 1998, Firoozabadi 1999).

Several specialized PVT experiments must be designed to tune the EOS and describe the phase behavior of CO2 correctly when it is mixed with the reservoir fluids. The lack of this information when CO2 flooding is simulated could lead to serious errors, as the incremental oil benefits are substantially dependent on the phase behavior and mass transfer calculations.

Some of the standard specialized PVT experiments conducted when CO2 injection is evaluated are the minimum miscibility pressure test (through slim-tube experiments or IFT method), Multiple Contact Experiments (backward or forward), Swelling tests, Interfacial Tension tests.

All the above experiments were carried out for the reference gas condensate field. The original gas condensate was obtained by recombining separator gas and oil samples at the initial GOR of M sand; then it was depleted at the reference pressure and constant reservoir temperature of 275°F. The reference was defined as the pressure at the time when the project could be implemented; the value was 4000 psi (below the saturation pressure). Equilibrium liquid condensate at 4000 psi was collected and then used for the experiments.

The executed experimental program was as follows:

- ✓ Compositional analysis of equilibrium condensate at 4000 psi.
- ✓ CCE of condensate at equilibrium at 275°F.
- ✓ 4-points of swelling with CO2 at 40, 80, 135, 172 % mol (% of the original condensate mols), swollen volume, density, and saturation pressure measured.
- ✓ CCE of each swelling point at 275°F.
- ✓ Viscosity measurement of each swollen mix at 275°F.
- ✓ Compositional analysis of the final mix (at 172% mol).
- ✓ Multi-contact test (5 contacts)

3.3 Equation of state model.

Before this reservoir simulation study, a 12 pseudo-component EOS model had been created using basic PVT and vaporizing experiments with lean gas. That model was useful to reproduce the fluid properties and phase behavior under depletion and lean gas injection strategies.
This EOS model was used to predict the new experimental tests with CO2. *Figure* 10-11 show the match between the experimental data of the swelling test and the EOS prediction. As observed in those figures, the EOS could not reproduce the results of the swelling test. Saturation pressures were overestimated, implying conservative benefits for CO2 injection. The miscibility and vaporizing mechanisms were not adequately represented.

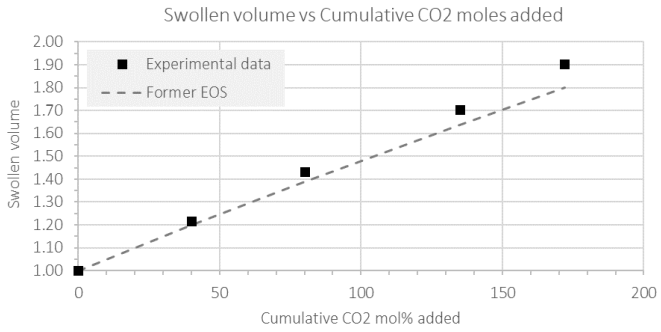

Figure 10. Experimental swollen volume versus simulated results for the swelling test with CO2.

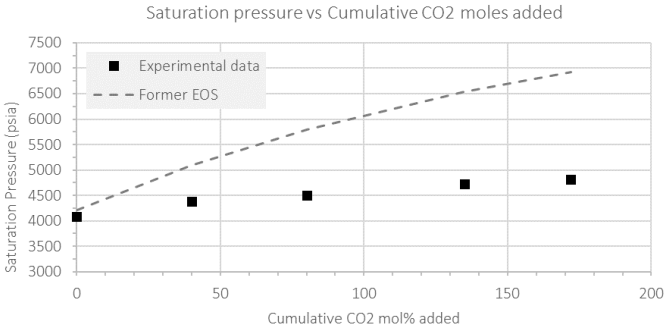

Figure 11. Experimental saturation pressure versus simulated results for the swelling test with CO2.

The mismatching of the former EOS was completely expected as the fluid model was created using only vaporization studies with lean gas, and it did not include CO2 injection tests.

To tune the equation of state with the new specialized PVT information, some regressions were set using the fluid simulator software Winprop of the CMG company. The interaction coefficients were selected as the regression parameters. Critical properties of the fluid model had already been calibrated with the former basic PVT and TBP studies from several wells; minimum changes were done for these parameters.

Figure 12*Figure* 18 show the match of the new EOS model with the experimental data. After multiple regressions, the new EOS model was obtained with a good match of all CO2 experimental data.

CCE of the condensate at equilibrium at 275°F:

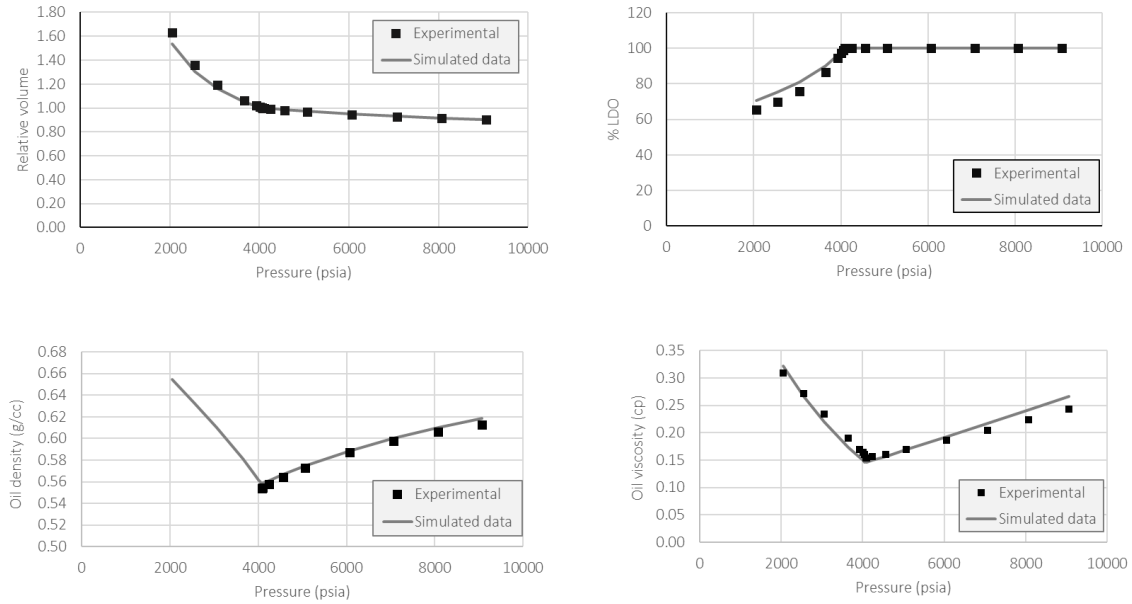

Figure 12. CCE of the condensate at equilibrium

4-points of swelling with CO2 at 40, 80, 135, 172 % mol

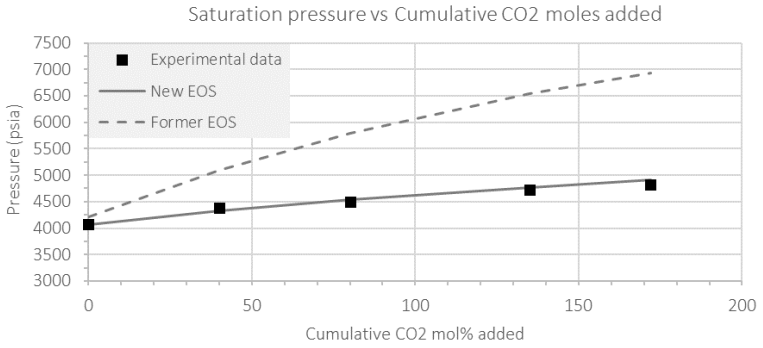

Figure 13. Experimental saturation pressure versus new EOS results for the swelling test with CO2.

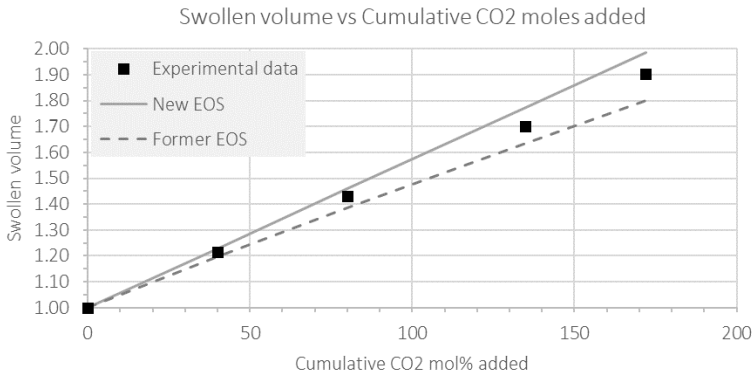

Figure 14. Experimental swollen volume versus new EOS results for the swelling test with CO2.

CCE of Mix-1 (40% mol) at 275°F:

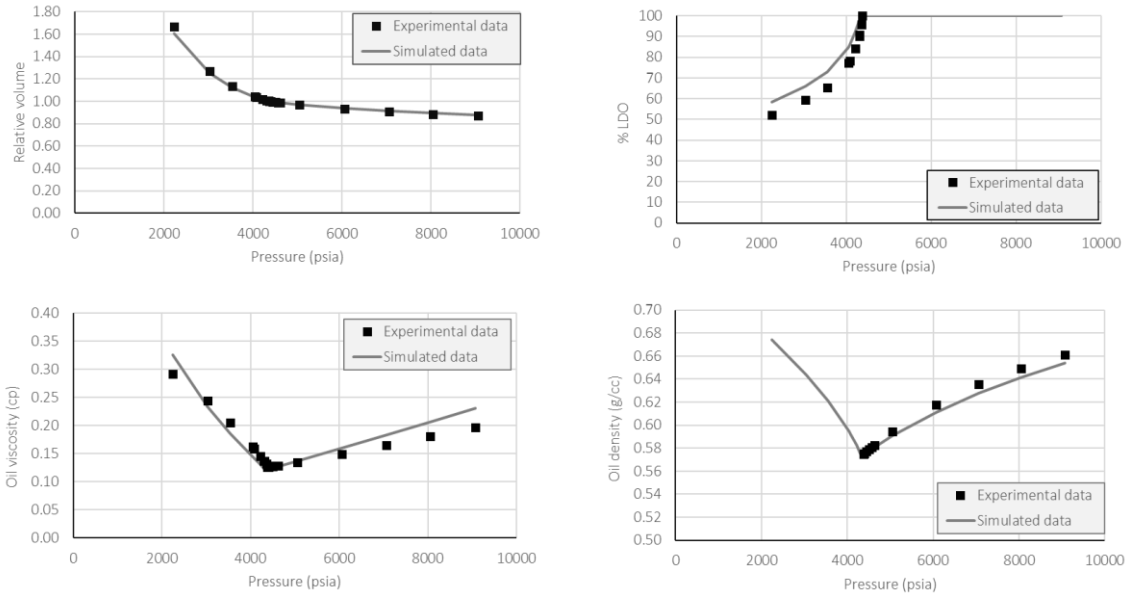

Figure 15. CCE of Mix-1. Comparison of simulated vs. observed data.

CCE of Mix-3 (135% mol) at 275°F:

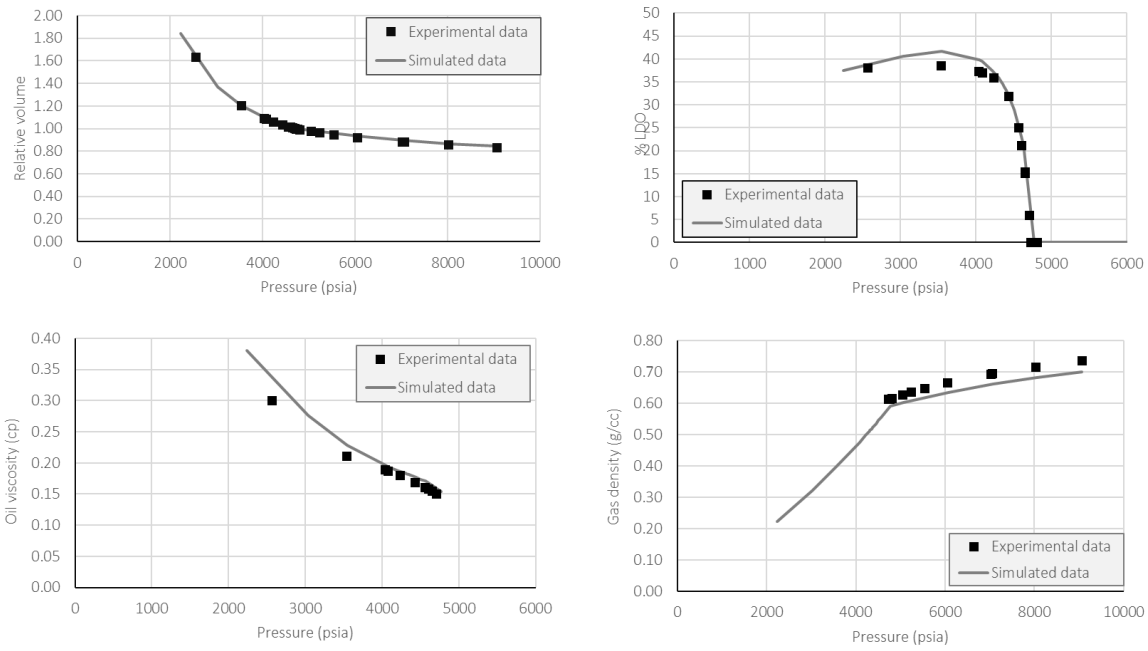

Figure 16. CCE of Mix-3. Comparison of simulated vs. experimental data.

Mix- D composition (172% mol added)

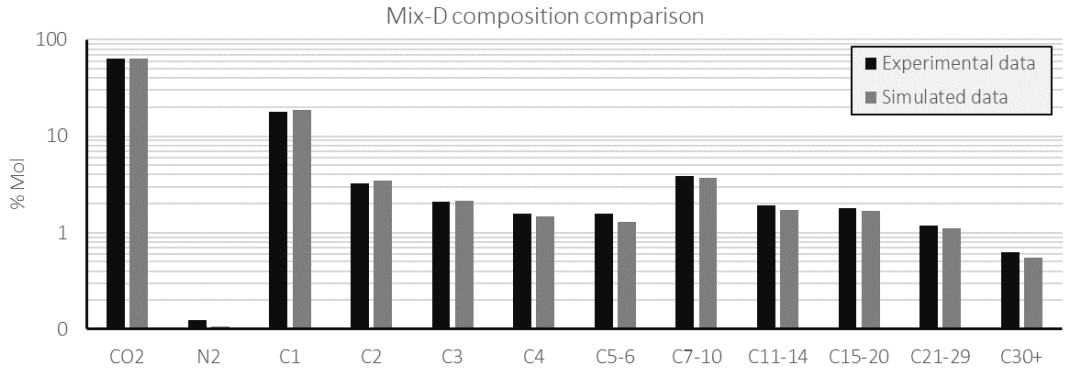

.

Figure 17. Mix-D composition, simulated vs. experimental data

Multi-contact test (5 contacts)

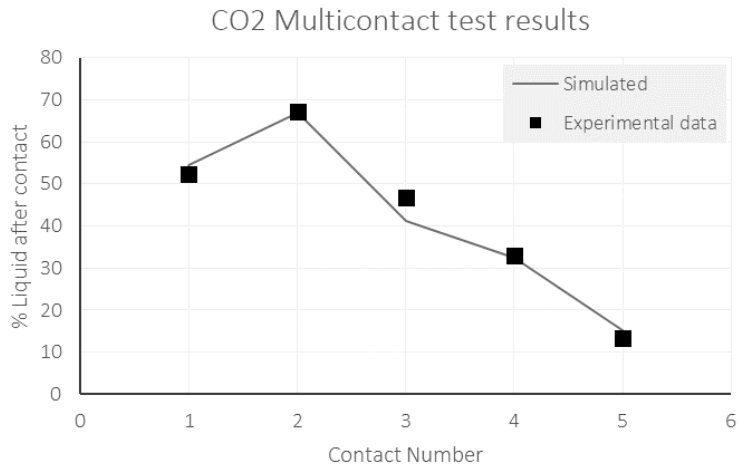

Figure 18. Simulated MCT vs. experimental data.

3.4 CO2 injection sensitivities

Multiple injection scenarios were set to evaluate the effects of CO2 injection rates and reservoir pressure in the condensate production and ultimate recovery. The evaluation of reservoir pressure was conducted with sensitivities varying the starting date of injection.

As mentioned in the above chapters, the injection was focused on the south zone of the M sand; only one well was evaluated as CO2 injector. *Figure 19* shows the oil saturation condition of the region in a 3D view, and the wells set up before injection.

Three constant CO2 rates were evaluated: 17, 25, and 35 MMscfd. All cases were run until the same date (estimated abandonment date).

For the reservoir pressure sensitivities, three dates were chosen as the starting date of injection: June of 2014, June of 2019 and June of 2024, which correspond to a reservoir pressure of 5250, 4650 and 4230 psia respectively. For each date, the above three rates were evaluated.

The evaluated reservoir pressures are below the dew point, and two phases are present in the rock: oil (condensate) and gas. The minimum miscibility pressure of the condensate (condensate liquid from the gas) was measured through IFT with the pendant drop method. The MMP was around

4550 psi; it means that in the first two scenarios the CO2 flooding is miscible with the condensate at the first contact (while pressure is kept above MMP)

The history match of the full field model was run until 2018. Nevertheless, as one of the objectives was to evaluate the injection at high reservoir pressures (2014 year), the Well-5 was constrained by THP from that date onwards instead of using real gas production. This condition was considered for all injection and natural depletion scenarios.

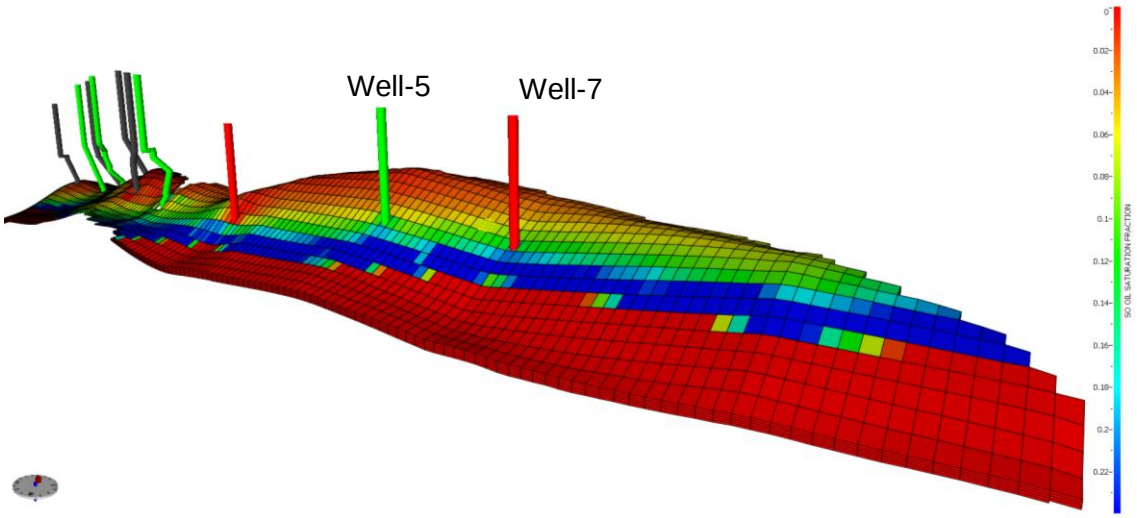

Figure 19. Oil saturation in a 3D view before CO2 injection.

3.5 Results and Discussion

This section presents the results of the simulated scenarios. The analysis was focused on the understanding of incremental oil production by well and field for each case, the oil recovery factor in the south region, the GOR evolution and CO2 breakthrough, the compositional changes in the gas and oil streams and on the integrated analysis of the scenarios.

3.5.1 Natural Depletion

In the natural depletion case, the calculated recovery factor for the south region at the abandonment date is 29.8 %, and the cumulative oil for the Well-5 is 18.2 MMbbl. *Figure 20* demonstrates the production behavior in terms of gas and oil rates, as well as the GOR and API trends for the Well-5. As it is observed, oil production presents an exponential decline of 1 % monthly and GOR exhibits and increasing trend as depletion occurs and the condensate from the

gas is left in the rock unrecoverable. Consequently, API continues the increasing trend observed in the historical data (*Figure 21*) as heavier components tend to condensate and stay in the reservoir. *Figure 22* shows the compositional changes of C7+ & C4-6 in the well-5 for the *do-nothing* case. As observed, intermediate hydrocarbons are produced and slowly increment in the oil stream.

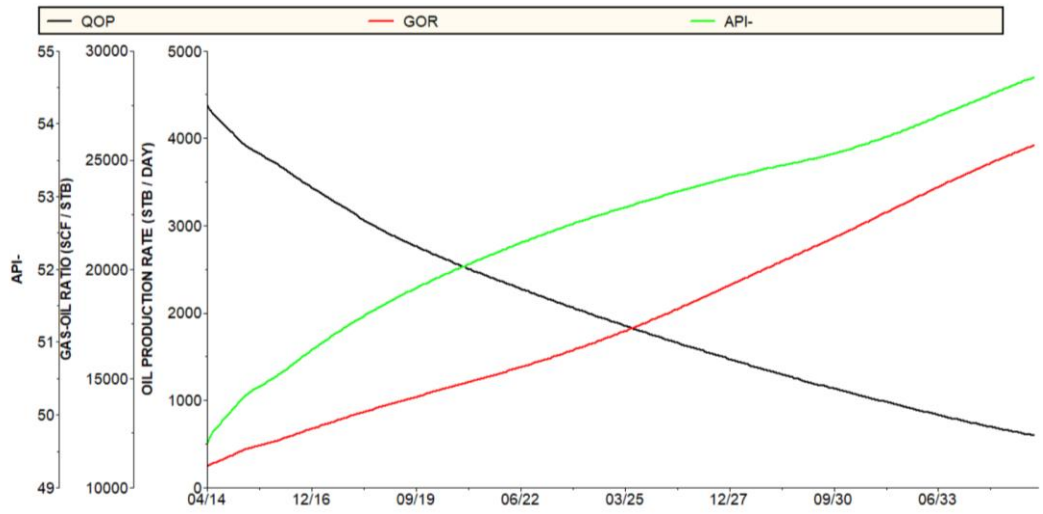

Figure 20. Production behavior for Well-5 in the *do-nothing* case.

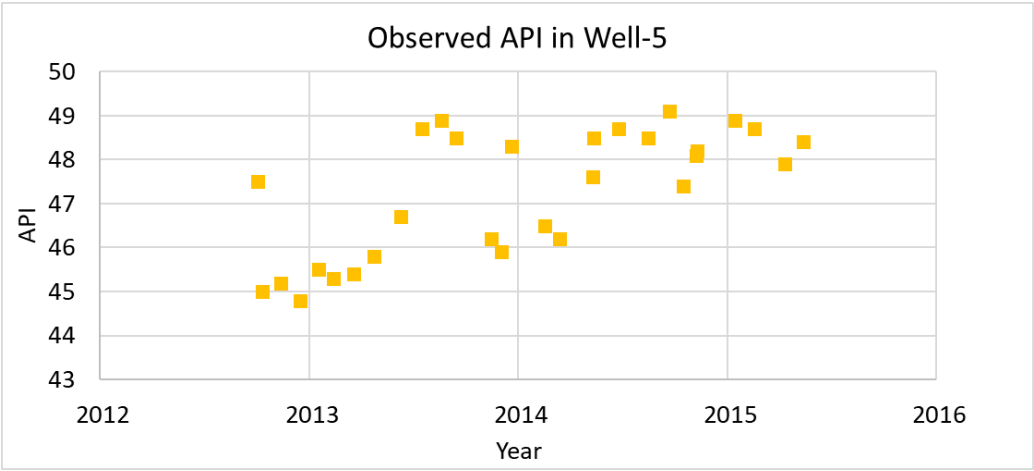

Figure 21. Observed API data for well-5.

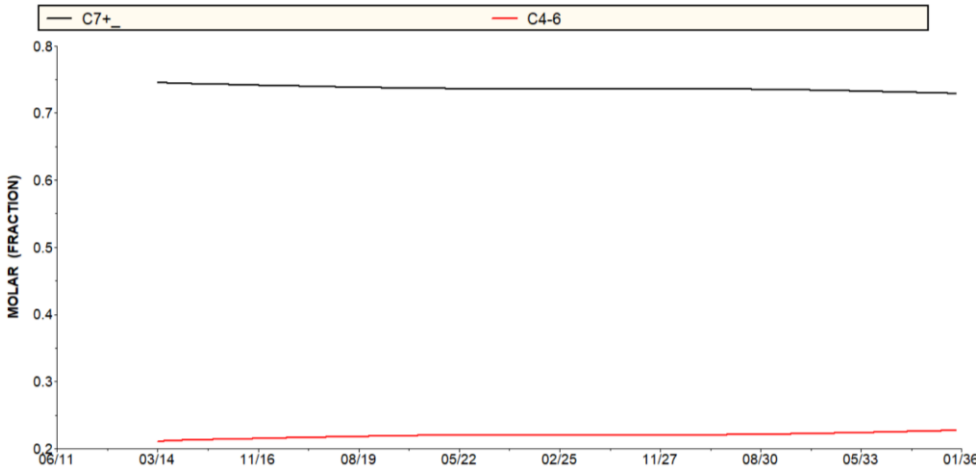

Figure 22. Compositional changes of C7+ & C4-6 in the well-5 for the *do-nothing* case.

Figure 23 demonstrates the condensate saturation that occurs in the near-wellbore of the producer well versus time. Condensate saturation increases as an effect of the reservoir depletion.

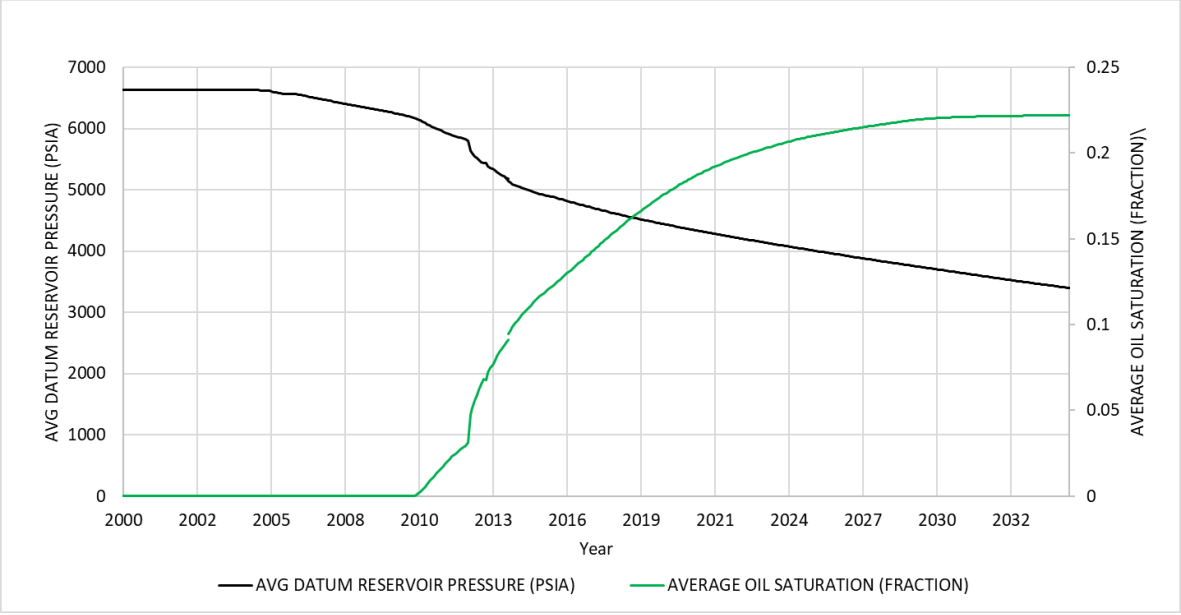

Figure 23. Condensate drop-out as depletion occurs for well-5.

3.5.2 Effects of CO2 Injection rates

In this section, the effects of injecting the following constant rates: 17, 25 and 35 MMscfd at a reservoir pressure of 5250 psia are analyzed (injection starting June 2014).

Figure 24-Figure 26 shows the oil and gas production profiles and GOR evolution. According to these figures, there is an improvement in oil production withing the first months of injection. The effect is reflected in the reduction of the oil decline rate (0.6% monthly for the case of 25 MMscfd versus 1 % of the depletion case). The incremental oil volume in the Well-5 is 2.7, 3.1, and 3.3 for the CO2 rates of 17, 25, and 35 MMscfd, respectively.

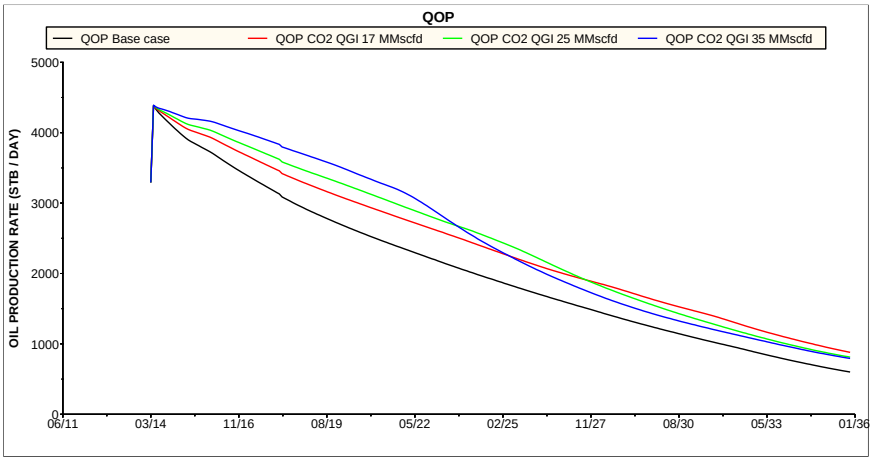

Figure 24. Oil production in Well-5 for the evaluated CO2 injection rates.

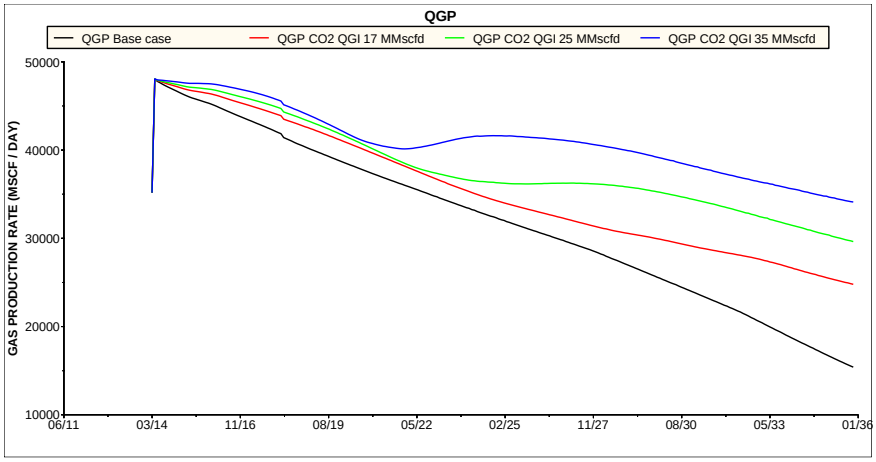

Figure 25. Gas production in Well-5 for the evaluated CO2 injection rates.

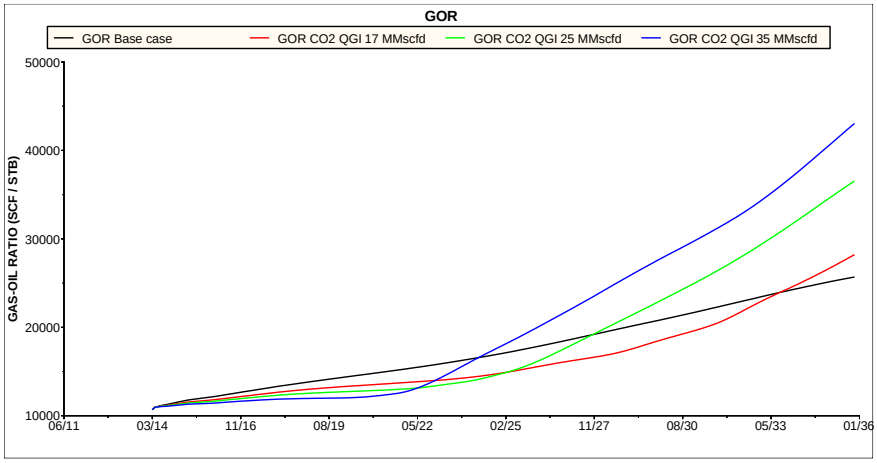

Figure 26. GOR trends in well-5 for the evaluated CO2 injection rates.

Figure 27 evidences the pressure support in the south region of M sand for the CO2 injection rates. The pressure decline trend is reduced from 0.17 % monthly in the depletion case to 0.12 % in the 25 MMscfd case.

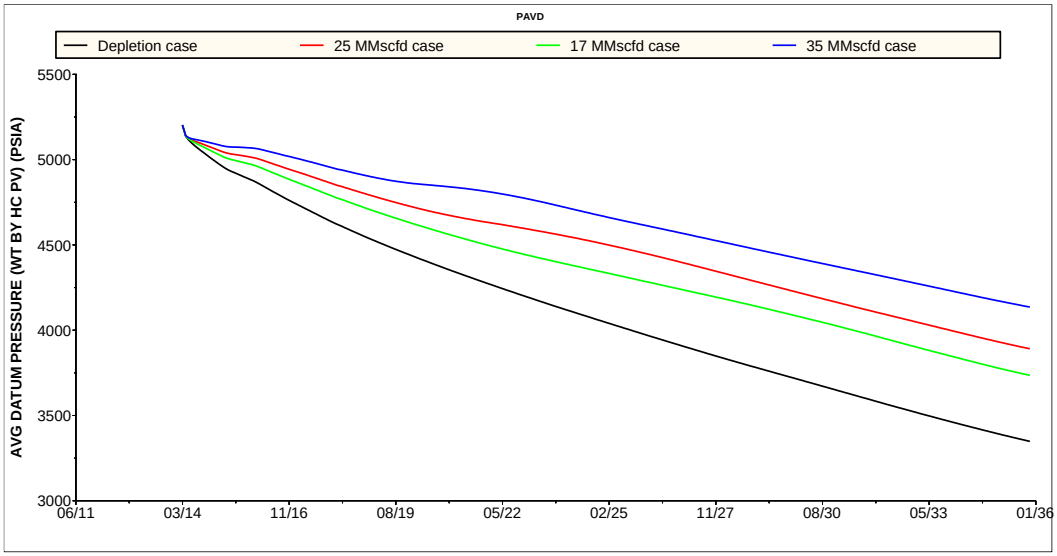

Figure 27. Reservoir pressure changes due to CO2 injection rates.

Figure 28*Figure* 32 compare the production behavior of the Well-5 for the injection case of 25 MMscfd versus the depletion scenario. According to these figures, the incremental oil production in the Well-5 due to the CO2 injection can be characterized by three different periods as follows:

I Period: Pressure support

The pressure support is the first mechanism that improves the condensate and gas production. The miscibility phenomenon occurs at the first contact if the reservoir pressure is above the MMP; otherwise, the mass transfer occurs between the CO2, the condensate, and gas phases. Beyond that region where these interactions take place, the original reservoir fluid is displaced by the injected mass, which increases the reservoir pressure.

This period is characterized by negligible compositional changes in the gas and oil streams. The remaining condensate in the rock that surrounds the producer well is reduced because of the reservoir pressure increment that consequently reduces the GOR trend in comparison to the depletion case. The API of the condensate continues increasing but not as much as in the depletion case.

Figure 28. C7+ in the produced condensate.

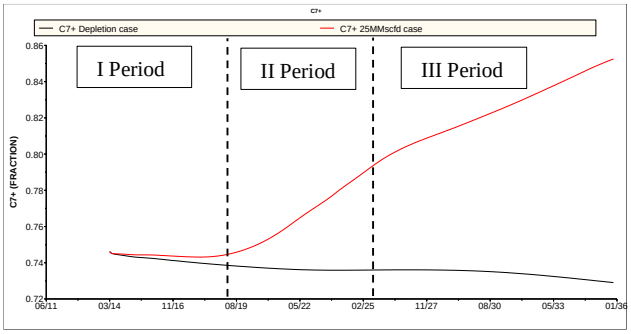

Figure 29. The CO2 content in the produced gas.

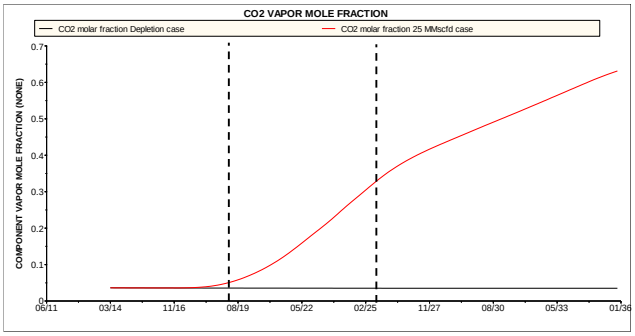

Figure 30. Average condensate saturation in the rock surrounding the producer well.

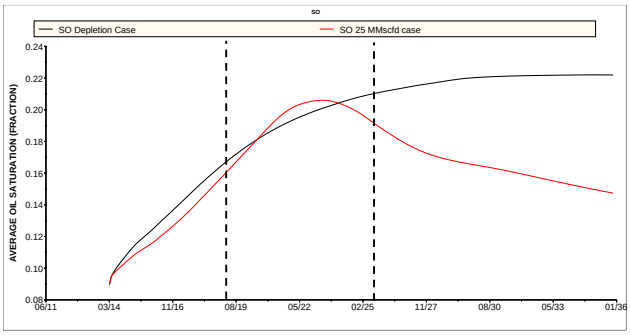

Figure 31. GOR evolution.

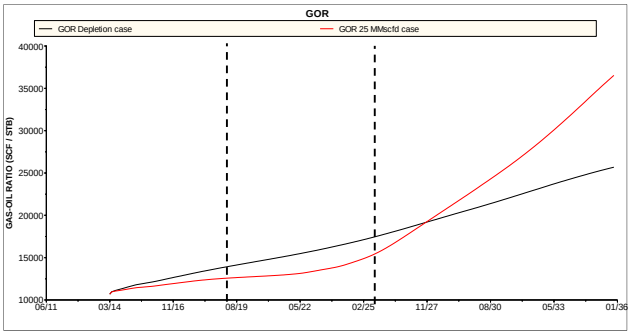

Figure 32. API trend.

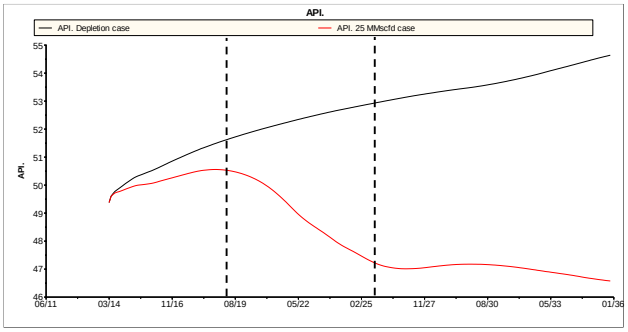

II Period: Rich gas condensate production

In this period, the initial CO2 breakthrough occurs; this is characterized by an increment of the CO2 content in the gas stream. The composition of the produced condensate changes as the CO2 vaporizes some quantity of it that was present in the rock because of the reservoir depletion. The C7+ fraction increases with time in the produced condensate and consequently, the API decreases. The CO2 front that is being produced is rich in intermediates and heavy components; it is observed in the flattening of the GOR trend.

Another observed phenomenon is the slight increment in the condensate saturation (So) around the producer wellbore in comparison with de depletion case, explained by the swelling mechanism

of the condensate oil in place that increases its volume and gives it some mobility. As the CO2 breakthrough continues, it vaporizes the condensate saturation around the producer wellbore.

III Period: CO2 Cycling

CO2 cycling is the last part of the flooding process. It is characterized by a strong GOR incremental trend as well as the increasing CO2 content in the gas stream. CO2 continues vaporizing the condensate in the rock around the producer wellbore (So decreases), and API remains low and relatively constant.

Figure 33 shows the oil recovery factor reached for the different rates. *Figure 34*-Figure 35 depict the GOR evolution and CO2 content in the Well-5 for the mentioned scenarios. According to *Figure 33*, the maximum recovery factor obtained is 38% when the reservoir pressure is 5250 psi, and the rate is 35 MMScfd.

The difference in the incremental oil volume for the Well-5 at the rates of 25 and 35 MMScfd, is negligible. This fact is due to the greater gas recycling that occurs with 35 MMScfd, evidenced in *Figure 34* with the early and strong increment in the GOR evolution and in *Figure* 35 with the increment of CO2 content in the gas production stream.

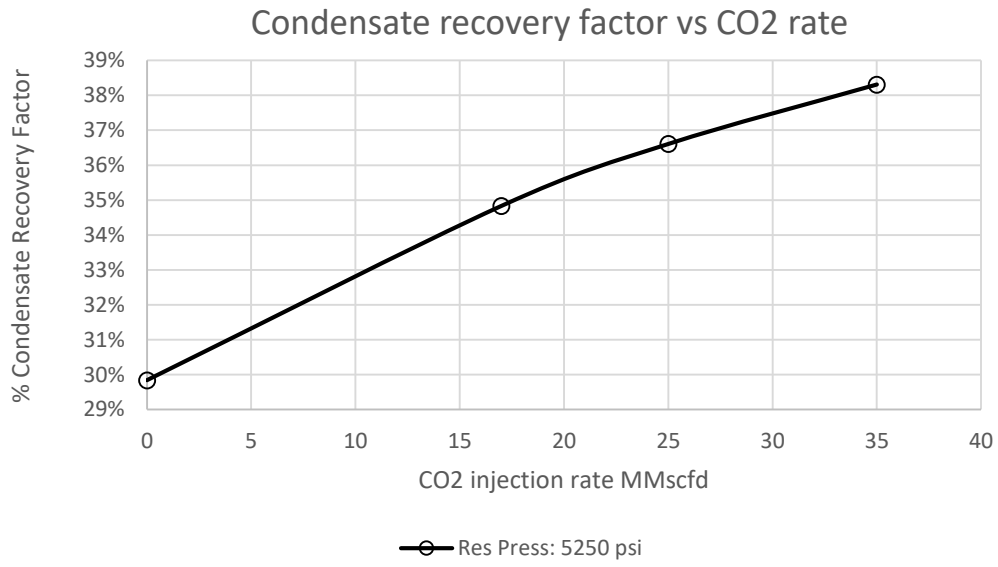

Figure 33. Condensate recovery factor concerning CO2 injection rates.

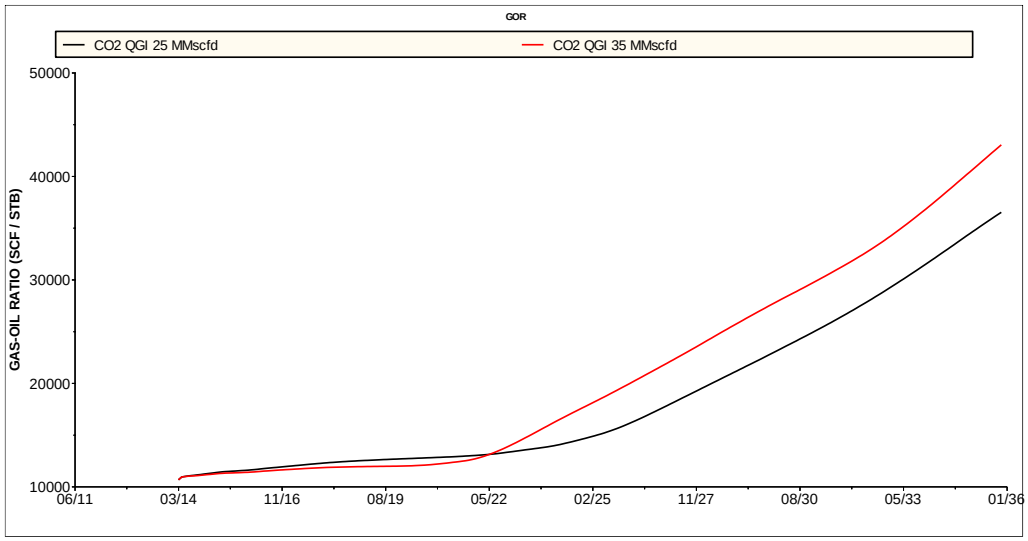

Figure 34. GOR trend of the Well-5 for 25 and 35 MMscfd cases.

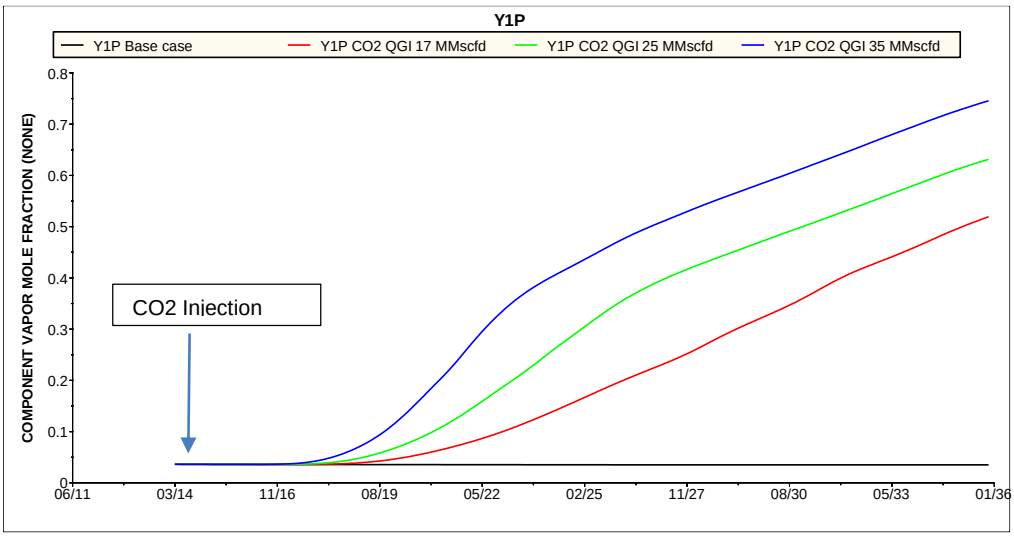

Figure 35. CO2 Molar fraction in the produced gas stream for the Well-5.

In addition to the benefits of the Well-5, some others wells in M-sand showed incremental oil due to the pressure support mechanism (CO2 content does not increase in the gas streams). The *Figure 36* shows the incremental oil volume at field level for the case when injection starts at a reservoir pressure of 5250 psi. According to *Figure 36*, the total incremental oil was 5.0, 6.7, and 8.6 MMbbls for 17, 25, and 35 MMscfd of injection, respectively.

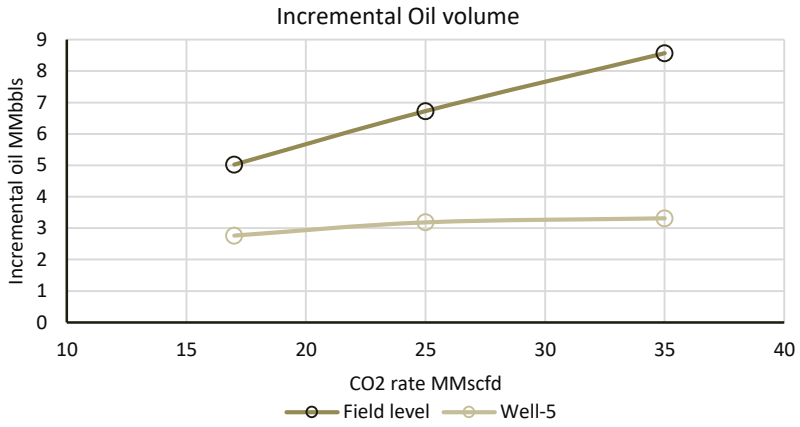

Figure 36. Incremental oil volume at field level for the case of Res P=5250 psi.

Figure 37-Figure 38 depict the months where the CO2 breakthrough occurs. As observed in *Figure 37-Figure 38*, the CO2 starts to be produced in the Well-5 after 60, 49 and 40 months of injecting 17, 25 and 35 MMScfd respectively.

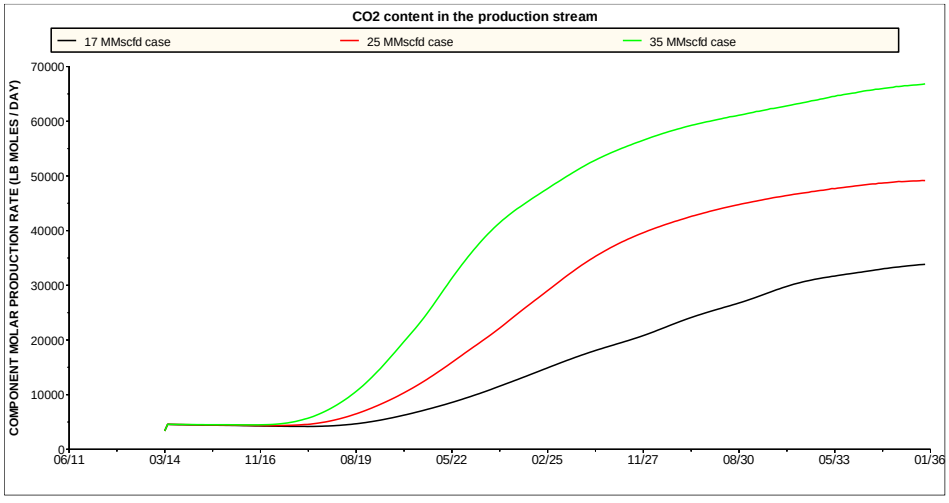

Figure 37. The CO2 content in the gas production stream of the well-5.

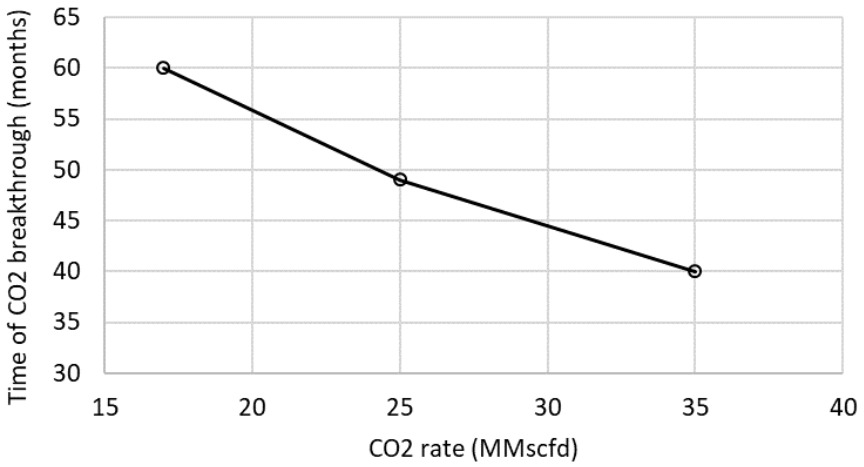

Figure 38. Time of CO2 breakthrough.

3.5.3 Effect of the reservoir pressure

For the reservoir pressure sensitivities, three dates were chosen for the start of injection: June of 2014, June of 2019 and June of 2024, which correspond to a reservoir pressure of 5250, 4650 and 4230 psia respectively. For each date, the above three rates were evaluated.

In all the cases, the reservoir pressure is below the saturation pressure and the quantity of condensate in the rock is higher as the depletion increases. *Figure 39* represents the condensate saturation in the region of the injector well before and after the injection for the 25 MMscfd case on different dates. According to *Figure 39*, the condensate saturation just before the injection is 0.14, 0.19 and 0.21 for 2014, 2019 and 2024 respectively.

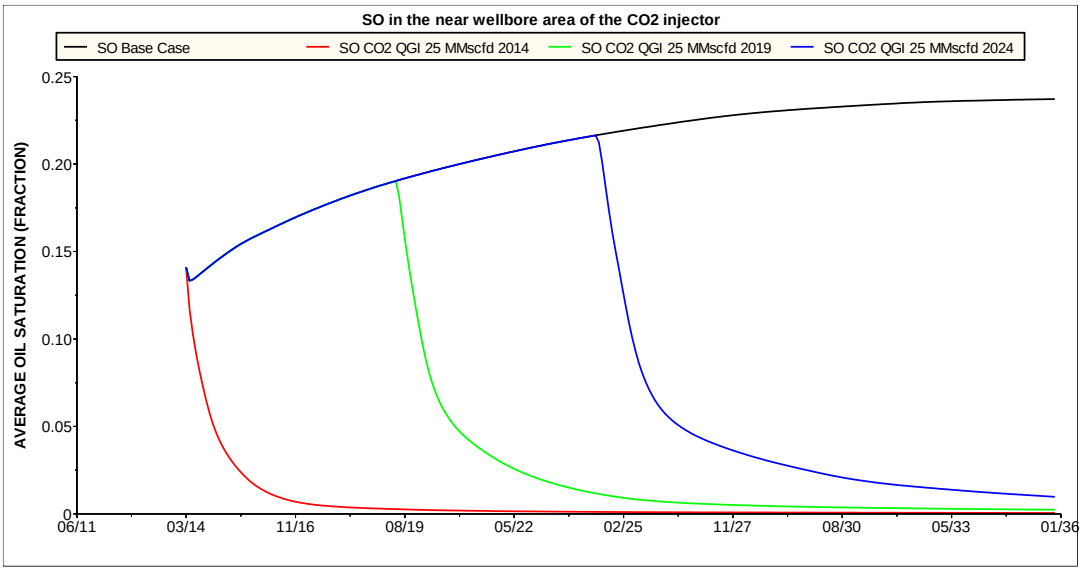

Figure 39. Condensate saturation in the region of the injector well before and after the injection for the 25 MMscfd case on different dates.

As observed in *Figure 39*, CO2 can vaporize most of the condensate saturation in place around the injector well, increasing the sweep efficiency. *Figure 40* shows the results of normalizing the condensate saturation profile in time to understand the effects of the reservoir pressure in the mass transfer phenomena. In *Figure 40*, all cases were plotted since the CO2 injection starts. It is interpreted that higher the reservoir pressure, faster and more efficient is the vaporization process.

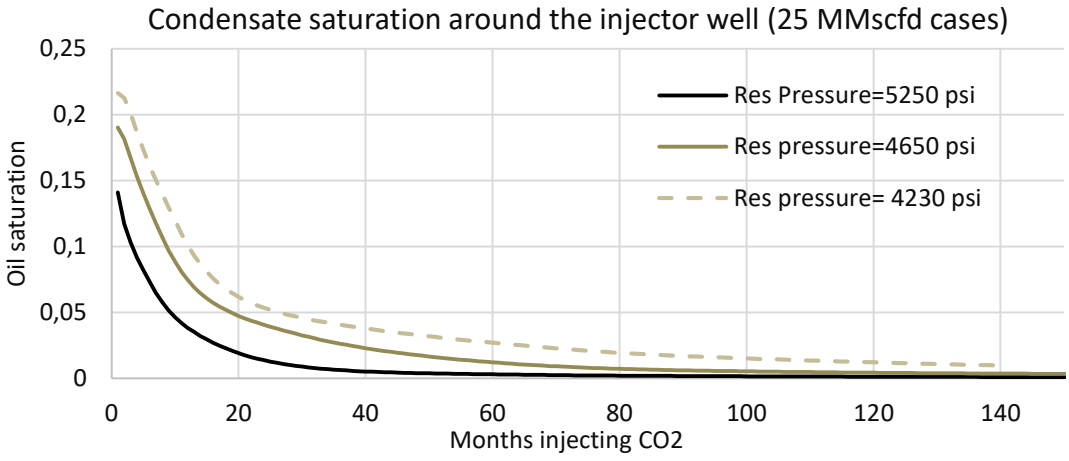

Figure 40. Normalized condensate saturation around the injector well for different reservoir pressures and 25 MMscfd of injection.

Figure 41Figure 42 show the oil saturation map of the region at the beginning and after seven years of the CO2 injection. According to *Figure 41Figure 42*, the CO2 can vaporize most of the contacted condensate in the reservoir.

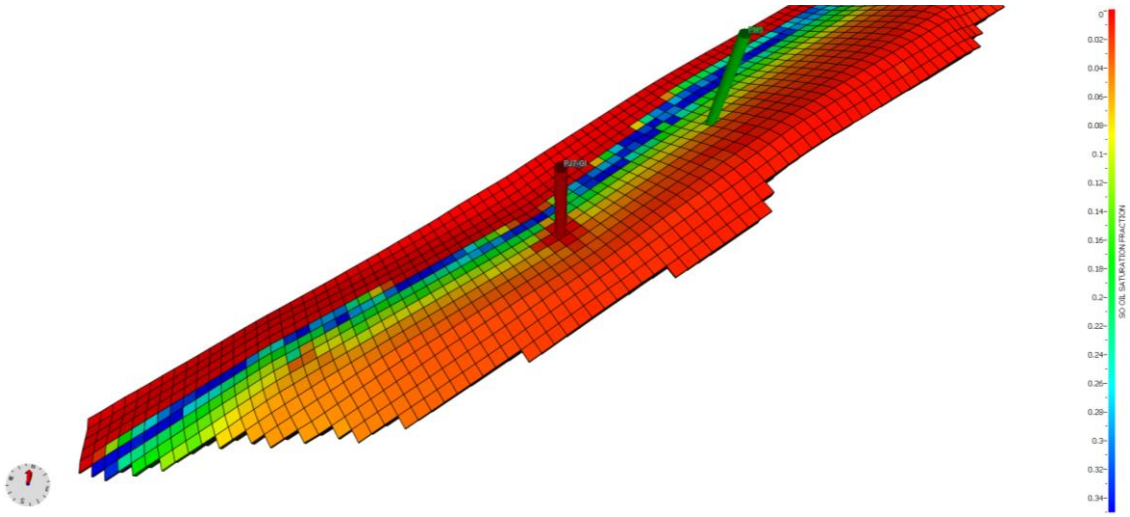

Figure 41. Oil saturation map at the beginning of the CO2 injection.

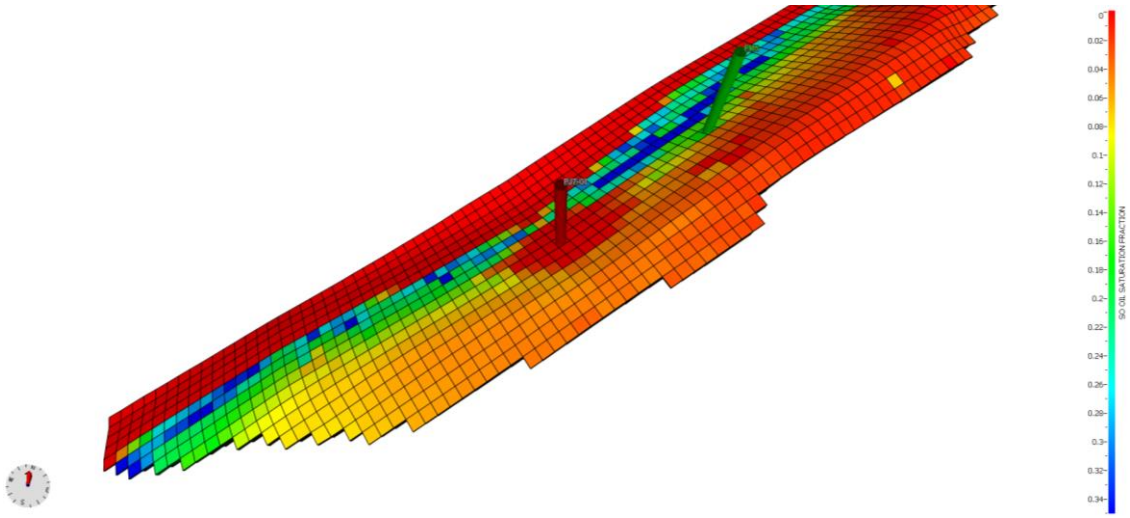

Figure 42. Oil saturation map after seven years of the CO2 injection.

Figure 43 presents the calculated incremental oil for Well-5. According to *Figure 43*, it is observed that lower the reservoir pressure, the less the incremental oil.

For the 35 MMscfd rate, the benefits in Well-5 were almost the same when injection started at a reservoir pressure of 5250 psi or 4650 psi. This is explained because of the higher recycling process that occurs at higher pressures where lower condensate saturation is present in the rock and gives more mobility to the CO2. Moreover, when the reservoir pressure is low, more condensate is present in the rock and reduce the CO2 mobility due to the relative permeability.

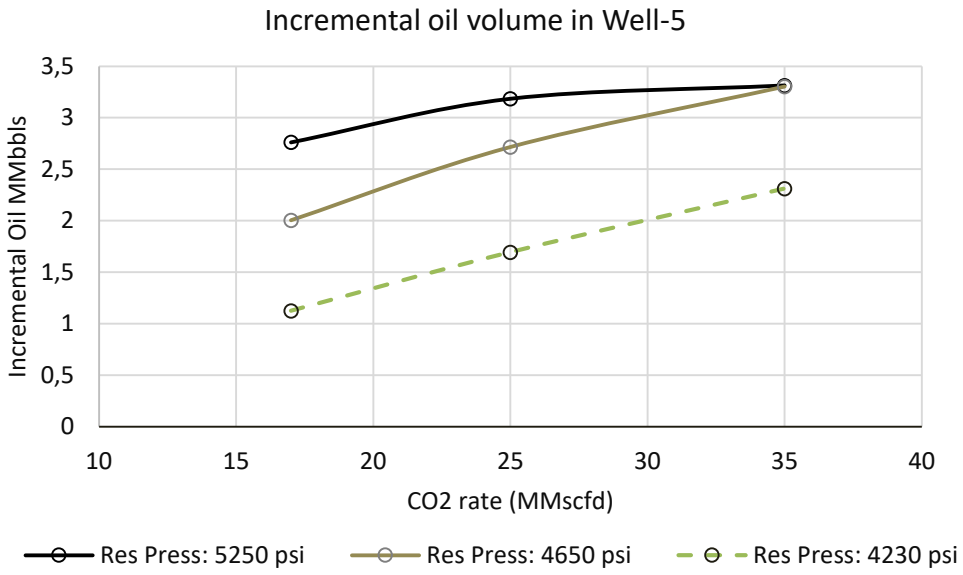

Figure 43. Incremental oil volume for the Well-5 at the different rates and reservoir pressure scenarios.

Figure 44 depicts the CO2 molar rate production, normalized since the CO2 breakthrough for the Well-5 and 35 MMscfd case. *Figure 45* shows the GOR trends for the reservoir pressures cases and 35 MMscfd of injection.

According to *Figure 44*, for the different reservoir pressure scenarios, it is possible to identify a higher CO2 production for the higher-pressure case in comparison to the lower-pressure scenario. Consequently, the GOR increases faster in the higher-pressure case as observed in *Figure 45*.

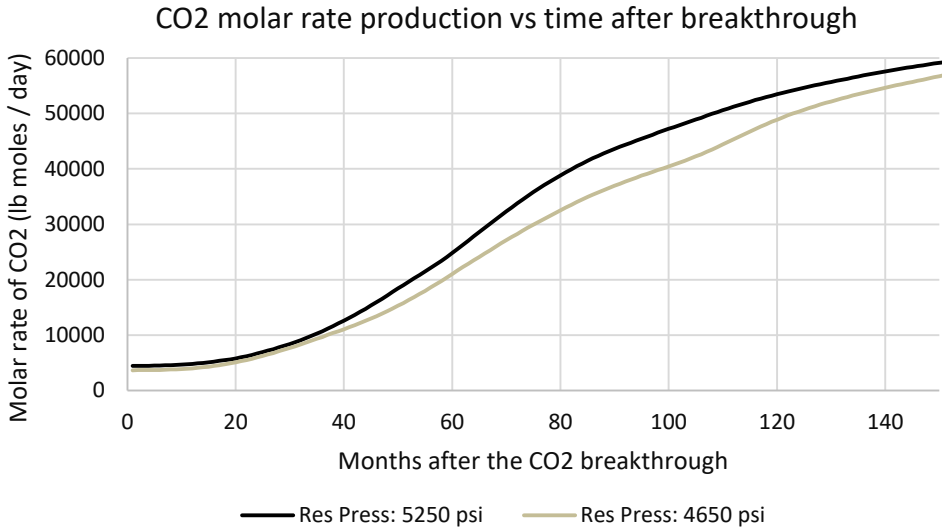

Figure 44. CO2 molar rate production, normalized since CO2 breakthrough for the Well-5 and 35 MMscfd case.

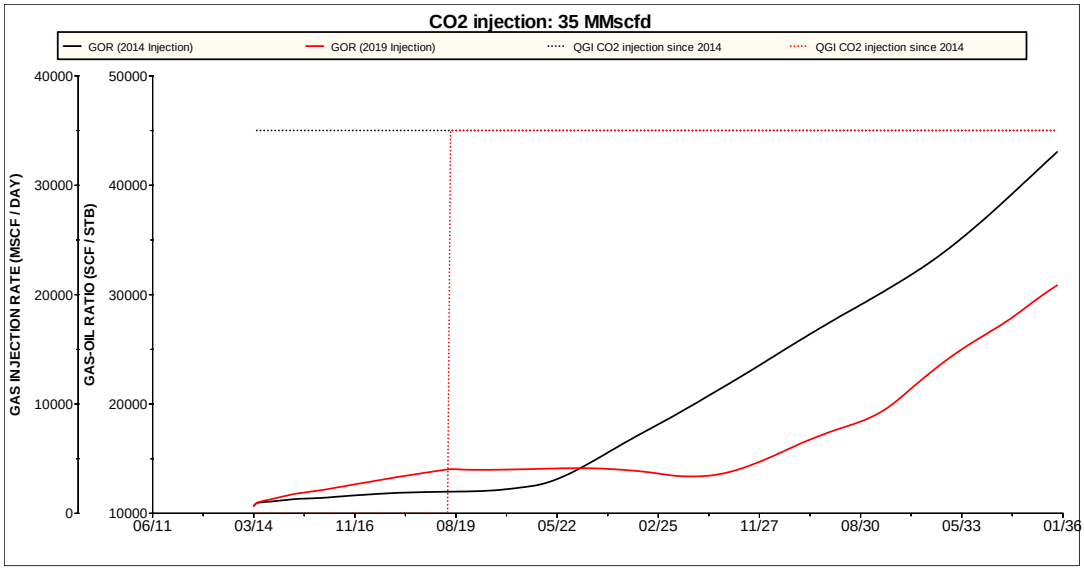

Figure 45. Comparison of the GOR trend after injecting 35 MMscfd in 2014 vs. 2019.

When the reservoir pressure is low, the condensate saturation increases in the rock. The CO2 injection under this scenario could vaporize a significant part of that saturation; then it is produced with the CO2 front, which becomes rich in intermediates and heavier components.

Figure 46 shows the injection case of 35 MMscfd at the reservoir pressure of 4230 psi. According to *Figure 46*, the pressure support mechanism is characterized by a stabilization of the GOR trend as less condensation occurs in the reservoir. The period of rich gas condensate production is characterized by a significant reduction in the GOR, an increment of CO2 content in the gas stream and a reduction of the API due to the production of intermediate and heavier components.

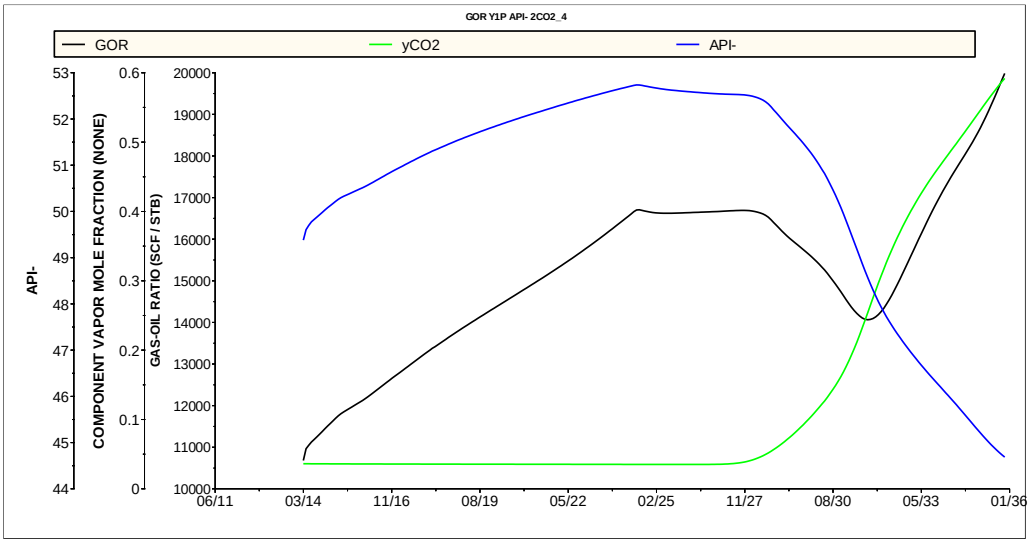

Figure 46. GOR, API & CO2 molar fraction for the Well-5 at a reservoir pressure of 4230 psi for the 35 MMscfd case.

Figure 47 presents the incremental oil volume at the field level. According to *Figure 47*, the reservoir pressure has a substantial impact on the incremental oil; CO2 flooding yields better results when it is executed at higher reservoir pressures. For the 25 MMscfd case, the incremental oil is 6.7, 4.2, and 2.1 MMbbls for the reservoir pressure of 5250, 4650, and 4230 psi respectively. It means a reduction in oil volume of 37% if the CO2 starts at a reservoir pressure of 4650 psi instead of 5260 psi, or a reduction of 68% if the CO2 starts at a reservoir pressure of 4230 psi.

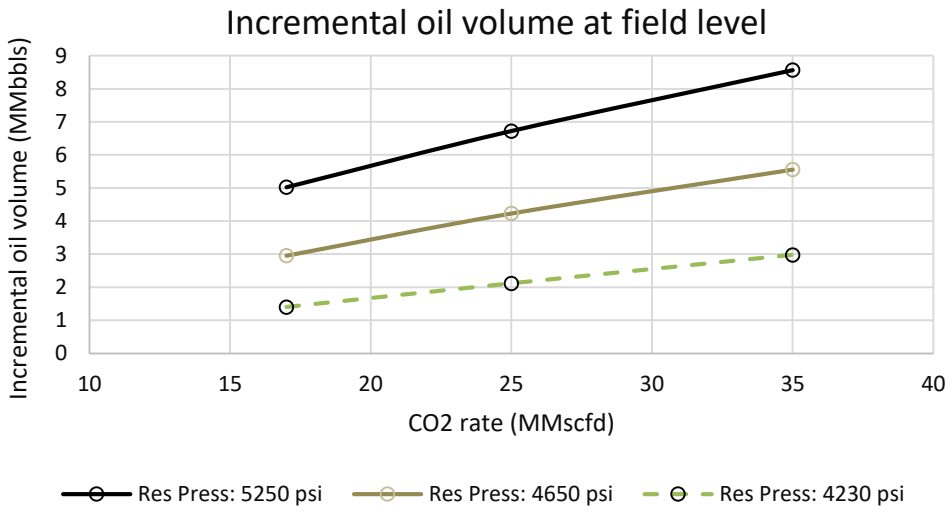

Figure 47. Incremental oil volume at field level for different rates and reservoir pressures sensitivities.

Figure 48 presents the oil recovery factor calculated for the different reservoir pressure scenarios. According to *Figure 48*, for the 25 MMscfd case, the condensate recovery factor was 33, 35 & 37% for a reservoir pressure of 5250, 4650, and 4230 psi, respectively.

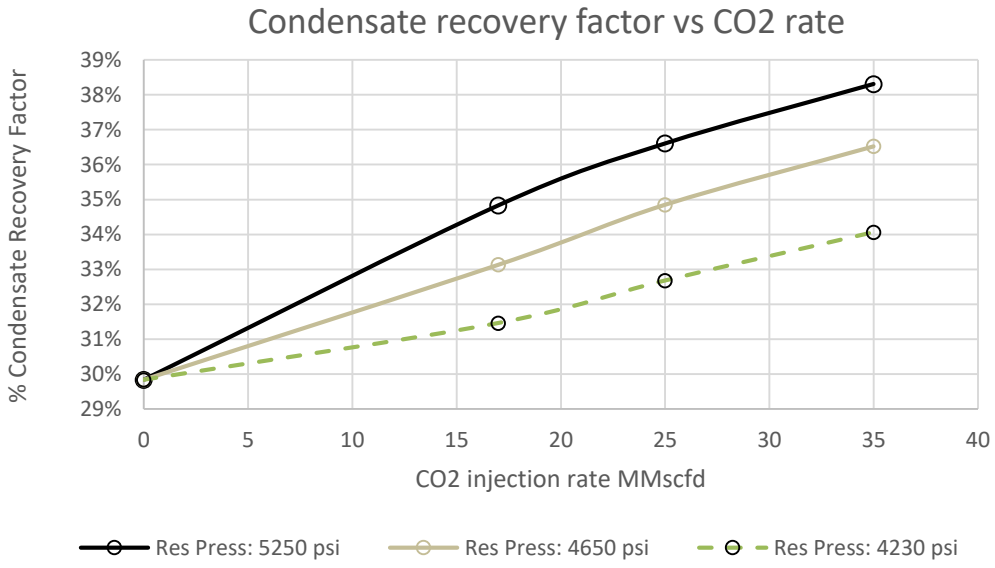

Figure 48. Condensate recovery factor at field level for different rates and reservoir pressures sensitivities.

CONCLUSIONS

A fully compositional multiphase flow model was used to evaluate the effects of CO2 injection into a gas condensate reservoir. The research objectives were to estimate the condensate recovery factor concerning different injection rates scenarios, the reservoir pressure effects in the condensate recovery efficiency, the compositional changes of the produced fluids and to understand the production mechanisms. The study concludes that:

- Several specialized PVT experiments must be designed to tune the EOS and describe the phase behavior of CO2 correctly when it is mixed with the reservoir fluids. The lack of this information when CO2 flooding is simulated could lead to serious errors, as the incremental oil benefits are substantially dependent on the phase behavior and mass transfer calculations.

- In the natural depletion case, the condensate recovery factor in the evaluated region would be 29.8%. The forecasted GOR of the producer well exhibits an increasing trend as depletion occurs and the condensate from the gas is left in the rock unrecoverable. Consequently, API increases as heavier molecules are left in the reservoir.

- The incremental oil production in the producer well due to the CO2 injection could be characterized by three different periods:

    - I Period: Pressure support

      The original reservoir fluid is displaced by the injected CO2 mass, which increases/maintains the reservoir pressure. This period is characterized by negligible compositional changes in the gas and oil streams. The remaining condensate in the rock that surrounds the producer well is reduced because of the reservoir pressure increment. Consequently, GOR evolution is reduced in comparison to the depletion case. The API of the condensate continues increasing but not as much as in the depletion case.

    - II Period: Rich gas condensate production

In this period, the initial CO2 breakthrough occurs; this is characterized by an increment of the CO2 content in the gas stream. The composition of the produced condensate changes as the CO2 vaporizes some quantity of it that was present in the rock because of the reservoir depletion. The C7+ fraction increases with time in the produced condensate and consequently, the API decreases. The CO2 front that is being produced is rich in intermediates and heavy components; it is observed in the flattening of the GOR trend.

- III Period: CO2 Cycling

  CO2 cycling is the last part of the flooding process. It is characterized by a strong GOR incremental trend as well as the increasing CO2 content in the gas stream. CO2 continues vaporizing the condensate in the rock around the producer wellbore (*So* decreases), and API remains low and relatively constant.

- Three constant injection rates were evaluated: 17, 25 & 35 MMscfd. The incremental oil at field level for a reservoir pressure of 5250 psi was 5.0, 6.7 and 8.6 MMbbls respectively. The benefits were observed not only by the main producer well but by the other wells in the M sand due to the pressure support. The condensate recovery factors for the evaluated region were 35, 37 and 38% for 17, 25 & 35 MMscfd respectively.

- The CO2 breakthrough occurred after 60, 49 and 40 months of injecting 17, 25 and 35 MMscfd, respectively.

- For the reservoir pressure sensitivities, three dates were chosen for the start of injection: June of 2014, June of 2019 and June of 2024, which correspond to a reservoir pressure of 5250, 4650 and 4230 psia respectively. CO2 could vaporize most of the condensate saturation in place around the injector well. The higher the reservoir pressure, the faster and more efficient was the vaporization processes.

- The reservoir pressure has a substantial impact on the incremental oil, CO2 flooding yields better results when it is executed at higher reservoir pressures (early in the field life). For the 25 MMscfd case, the incremental oil is 6.7, 4.2, and 2.1 MMbbls for the reservoir pressure of 5250, 4650, and 4230 psi respectively. It means a reduction in oil volume of 37% if the CO2 starts at a reservoir pressure of 4650 psi instead of 5260 psi, or a reduction of 68% if the CO2 starts at a reservoir pressure of 4230 psi.

- For the 25 MMscfd case, the condensate recovery factor was 33, 35 & 37% for a reservoir pressure of 5250, 4650, and 4230 psi respectively.

- When CO2 injection started at high reservoir pressure, the quantity of liquid condensate in the rock was small. This condition gave to the CO2 more mobility considering the relative permeability curves in comparison to the lower pressure case where higher condensate saturation was present in the rock. GOR increases faster as higher the reservoir pressures.

REFERENCES

Al-Abri, A. S. (2011). Enhanced Gas Condensate Recovery by CO2 Injection (Doctoral dissertation, Curtin University of Technology). Retrieved from https://espace.curtin.edu.au/bitstream/handle/20.500.11937/1770/159514_Al-Abri2011.pdf?sequence=2&isAllowed=y

Brown, J. S. (2014). *A Compositional Simulation Model For Carbon Dioxide Flooding With Improved Fluid Trapping* (Doctoral dissertation, Colorado School of Mines). Retrieved from https://mountainscholar.org/bitstream/handle/11124/17037/Brown_mines_0052E_10621.pdf?sequence=1&isAllowed=y

Cadogan, S. P. (2015). *Diffusion of CO2 in Fluids Relevant to Carbon Capture, Utilisation and Storage* (Doctoral dissertation, Imperial College London). Retrieved from https://core.ac.uk/download/pdf/77007460.pdf

Carbon capture & sequestration technologies – MIT. (2016). Denver Unit Fact Sheet: Commercial EOR using Anthropogenic Carbon Dioxide. Retrieved from https://sequestration.mit.edu/tools/projects/denver_unit.html

Computer Modelling Group. (2015). Gem User Guide Compositional & Unconventional Reservoir Simulator. Calgary, Alberta. Retrieved from https://www.studocu.com/en/document/university-of-oxford/machine-learning/tutorial-work/cmg-gem-user-guide-2014/1613556/view

Crotti, M. A., Cobenas, R. H. (2001). Scaling Up of Laboratory Relative Permeability Curves. An Advantageous Approach Based on Realistic Average Water Saturations. *Society of Petroleum Engineers.* doi:10.2118/69394-MS.

Darvish, G. (2007). *Physical Effects Controlling Mass Transfer in Matrix Fracture System During CO2 Injection into Chalk Fractured Reservoirs* (Doctoral dissertation, Norwegian University of Science and Technology). Retrieved from https://ntnuopen.ntnu.no/ntnu-xmlui/bitstream/handle/11250/239279/122941_FULLTEXT01.pdf?sequence=1&isAllowed=y

Garcia, M. (2005). *Optimization of a CO2 Flood Design Wasson Field - West Texas* (Master´s thesis, Texas A&M University). Retrieved from https://core.ac.uk/download/pdf/4271109.pdf

Gharbia, I. B., Flauraud, E., & Michel, A. (2015). Study of Compositional Multi-Phase Flow Formulations with Cubic EOS. *Society of Petroleum Engineers*. doi:10.2118/173249-MS.

Global Energy Statistical Yearbook. (2019). World Energy Statistics. Retrieved from https://yearbook.enerdata.net/

Herrera, C. (2016). *Simulation of Nitrogen Injection as an Enhanced Recovery Method in a Tight Natural Fracture Sandstone Reservoir with Compositional Fluids* (Master´s thesis, Universidad Nacional de Colombia). Retrieved from http://bdigital.unal.edu.co/53175/1/75090447.2016.pdf

Hoteit, H. (2011). Proper Modeling of Diffusion in Fractured Reservoirs. *Society of Petroleum Engineers*. doi:10.2118/141937-MS.

Kane, A. V. (1979). Performance Review of a Large-Scale CO2-WAG Enhanced Recovery Project, SACROC Unit Kelly-Snyder Field. *Society of Petroleum Engineers*. doi:10.2118/7091-PA.

Leahy-Dios, A., Firoozabadi, A. (2007). Unified Model for Nonideal Multicomponent Molecular Diffusion Coefficients. *The Global Home of Chemical Engineers.* doi*:* 10.1002/aic.11279

Moortgat, J., Firoozabadi, A. (2013). Fickian Diffusion in Discrete-Fractured Media from Chemical Potential Gradients and Comparison to Experiment. *Energy Fuels.* 2013; 27:5793-5805.

Occidental petroleum. (2015). Oxy Denver Unit CO2 Subpart RR. Retrieved from https://www.epa.gov/sites/production/files/201512/documents/denver_unit_mrv_plan.pdf

Ren, S., Niu, A., Ren, B., Li, Y., Kang, W., Chen, G. Zhang, H. (2011). Monitoring on CO2 EOR and Storage in a CCS Demonstration Project of Jilin Oilfield China. *Society of Petroleum Engineers*. doi:10.2118/145440-MS

Rodriguez, F., & Galindo-Nava, A. (1994). A General Formulation for Compositional Reservoir Simulation. *Society of Petroleum Engineers*. doi:10.2118/28705-MS.

S.A.S., E. (2019). Reservas de petróleo llegaron a 1.958 millones de barriles en 2018. Retrieved from https://www.larepublica.co/economia/reservas-de-petroleo-en-colombia-2018-2861481

Schmall, L., Varavei, A., & Sepehrnoori, K. (2013). A Comparison of Various Formulations for Compositional Reservoir Simulation*. Society of Petroleum Engineers*. doi:10.2118/163630-MS.

Tabrizy, V. A. (2012). *Investigated Miscible CO2 Flooding for Enhancing Oil Recovery in Wettability Altered Chalk and Sandstone Rocks* (Doctoral dissertation, University of Stavanger).

TNO. (2019). K12-B, CO2 storage and enhanced gas recovery. Retrieved from https://www.tno.nl/media/1581/357beno.pdf

UPME. (2017). Balance de Gas Natural 2017. Retrieved from http://www1.upme.gov.co/Hidrocarburos/publicaciones/Balance_Gas_Natural_2017-2026_26122017_VF.pdf

U.S. Department of the Interior: U.S. Geological Survey. (2015). *Fundamentals of Carbon Dioxide-Enhanced Oil Recovery (CO2-EOR)—A Supporting Document of the Assessment Methodology for Hydrocarbon Recovery Using CO2-EOR Associated with Carbon Sequestration.* Retrieved from https://pubs.usgs.gov/of/2015/1071/pdf/ofr2015-1071.pdf

U.S. Department of the Interior: U.S. Geological Survey. (2017). *Carbon Dioxide Enhanced Oil Recovery Performance According to the Literature*. Retrieved from https://pubs.usgs.gov/sir/2017/5062/d/sir20175062_chapd.pdf

Wang, H., Ewing, R., Qin, G., & Lyons, S. L. (2006). An Eulerian-Lagrangian Formulation For Compositional Flow In Porous Media. *Society of Petroleum Engineers*. doi:10.2118/102512-MS

Whitson, C. H., Brulé, M. R. (2000). *Phase Behavior* (Monograph Volume 20 Spe Henry L. Doherty Series edn.). Texas, SPE Monograph Series.